REPUBLIC OF TURKEY

YILDIZ TECHNICAL UNIVERSITY

GRADUATE SCHOOL OF NATURAL AND APPLIED SCIENCES

DEVELOPMENT AND INVESTIGATION OF WHITE LIGHT EMITTING DIODES WITH BLUE EMITTING CARBON DOTS-COATED DYSPROSIUM DOPED LUMINESCENT GLASSES

Beyza ÖZLEM

MASTER OF SCIENCE THESIS

Department of Metallurgical and Materials Engineering

Materials Program

Supervisor

Assoc. Prof. Dr. Miray ÇELİKBİLEK ERSUNDU

August, 2023

REPUBLIC OF TURKEY

YILDIZ TECHNICAL UNIVERSITY

GRADUATE SCHOOL OF NATURAL AND APPLIED SCIENCES

DEVELOPMENT AND INVESTIGATION OF WHITE LIGHT EMITTING DIODES WITH BLUE EMITTING CARBON DOTS-COATED DYSPROSIUM DOPED LUMINESCENT GLASSES

A thesis submitted by Beyza ÖZLEM in partial fulfillment of the requirements for the degree of MASTER of SCIENCE is approved by the committee on 04.08.2023 in Department of Metallurgical and Materials Engineering.

Assoc. Prof. Dr. Miray ÇELİKBİLEK ERSUNDU
Yıldız Technical University
Supervisor

Approved By the Examining Committee

Assoc. Prof. Dr. Miray ÇELİKBİLEK ERSUNDU, Supervisor
Yildiz Technical University _____

Assoc. Prof. Dr. Fatih AKYOL, Member
Yildiz Technical University _____

Prof. Dr. Esra ÖZKAN ZAYİM, Member
Istanbul Technical University _____

I hereby declare that I have obtained the required legal permissions during data collection and exploitation procedures, that I have made the in-text citations and cited the references properly, that I haven't falsified and/or fabricated research data and results of the study and that I have abided by the principles of the scientific research and ethics during my Thesis Study under the title of Development and Investigation of White Light Emitting Diodes with Blue Emitting Carbon Dots-coated Dysprosium Doped Luminescent Glasses supervised by my supervisor, Assoc. Prof. Dr. Miray ÇELİKBİLEK ERSUNDU. In the case of a discovery of false statement, I am to acknowledge any legal consequence.

Beyza ÖZLEM

Signature

This study was supported by The Scientific & Technological Research Council of Turkey (TUBITAK) under project numbered 119C025 and Yildiz Technical University Scientific Research Projects Coordination Unit under project number FBA-2022-4999.

To be worthy does not mean to be perfect…

ACKNOWLEDGEMENTS

I am deeply grateful to my supervisor, Assoc. Prof. Dr. Miray ÇELİKBİLEK ERSUNDU, for her exceptional supervision and guidance throughout this study. Her expertise and dedication have been instrumental in shaping the success of my research. She consistently provided valuable insights, constructive feedback, and unwavering support that greatly contributed to the quality and depth of my work. Her mentorship extended far beyond this study, as she has been a constant source of support and encouragement throughout my entire education as an engineer. I would also like to express my heartfelt appreciation to Assoc. Prof. Dr. Ali Erçin ERSUNDU for his invaluable guidance and assistance during my entire period as a student. His wealth of knowledge, patience, and willingness to share his expertise have been instrumental in my academic growth. Moreover, I would like to acknowledge the trust that both Assoc. Prof. Dr. Miray ÇELİKBİLEK ERSUNDU and Assoc. Prof. Dr. Ali Erçin ERSUNDU placed in me by giving me the opportunity to be a part of their research group. Their confidence in my abilities to conduct independent research has been empowering.

I would like to extend my sincere appreciation to the former and current members of the YTU Glass Research Group for making this journey an enjoyable one. Their camaraderie and support have been invaluable throughout my experience. First and foremost, I would like to express my deepest gratitude to Dr. Erdinç EROL for his exceptional guidance and unwavering support, especially during times when the results were not as expected. His mentorship and encouragement have played a significant role in my growth as a researcher and not only helped me navigate through obstacles but also instilled in me a sense of resilience and determination to overcome any challenges that came my way. I also want to acknowledge Dr. Orhan KIBRISLI for his significant role in my development, elevating me from a junior member to a senior researcher, and eventually allowing me to ‘unofficially’ lead the lab. I am grateful for the opportunity to pursue his legacy and contribute to the growth of the lab. I cannot forget to mention my partner in crime, Ulaş KORKMAZ. From the beginning of this journey until now, we have shared numerous experiences, both joyful and challenging. Despite our current paths diverging, I am grateful for the long way we have come together, supporting each other through tears and laughter. Furthermore, I would like to express my appreciation to M.Sc Naji

VAHEDİ for his visual intelligence and the interesting moments he creates seemingly out of nowhere. Your creativity and contributions have added a distinct flavor to our research group. Lastly, I extend my gratitude to Utku EEKİM, the tall young guy, even though your work ethic sometimes got on my nerves, thank you for making sure that I ate properly. To all those mentioned, and to the entire YTU Glass Research Group, I am incredibly grateful for the memories, experiences, and the sense of belonging that we have shared. Your contributions and support have made this journey truly memorable.

I would like to thank The Scientific & Technological Research Council of Turkey (TUBITAK) for their financial support under project numbered 119C025 and Yildiz Technical University Scientific Research Projects Coordination Unit for their financial support under project number FBA-2022-4999.

In addition to expressing my gratitude to my colleagues, I would like to extend my heartfelt appreciation to my family for their unwavering support and unconditional love. They have been a constant source of encouragement and strength throughout my extended education and research journey. To my father, Erman, and my sister, Eda, I am deeply grateful for their unending support. They have stood by me without hesitation, offering words of encouragement and understanding during the challenging moments. Their belief in my abilities has been a driving force behind my perseverance, and I am truly fortunate to have such loving and supportive family members. I would also like to express my profound gratitude to my dearest mother, Lütfiye, who dedicated herself to raising me until her last breath and watches over me from heaven. From the very beginning, she instilled in me a sense of determination and resilience, and I could always sense her presence. Whenever I felt lost or overwhelmed, she would show me the white butterfly as a symbol of hope and assurance that there was always a way out. Even in her absence, her love and influence continue to shape my journey, and I carry her memory in my heart as a constant source of inspiration.

Beyza ÖZLEM

TABLE OF CONTENTS

ACKNOWLEDGEMENTS **v**
TABLE OF CONTENTS **vii**
LIST OF SYMBOLS **ix**
LIST OF ABBREVIATIONS **x**
LIST OF FIGURES **xi**
LIST OF TABLES **xiv**
ABSTRACT **xv**
ÖZET **xvii**
1 INTRODUCTION **1**
1.1 Literature Review ... 1
1.2 Objective of Thesis ... 2
1.3 Hypothesis ... 2
2 THEORETICAL INFORMATION **4**
2.1 Energy and Solid-State Lighting Technologies ... 4
2.2 Luminescence ... 6
2.2.1 Photoluminescent Materials ... 9
2.2.2 Down-Conversion Mechanism of Dy^{3+} ... 10
2.2.3 Fluorescence Mechanism of Carbon Dots ... 11
2.2.4 White Light Emission from Down-Conversion ... 13
3 EXPERIMENTAL STUDIES **15**
3.1 Sample Synthesis ... 15
3.1.1 Luminescent Glass Synthesis ... 15
3.1.2 Blue Carbon Dots and BCDs/PVP Solution Synthesis ... 17
3.1.3 The Coating Process ... 18
3.2 Sample Characterization ... 20
3.2.1 Structural Analysis ... 20
3.2.2 Thermal Analysis ... 21
3.2.3 Optical Analysis ... 21
3.2.4 Chemical Analysis ... 22
3.2.5 Morphological Analysis ... 22
3.2.6 Photoluminescent Analysis ... 23
3.2.7 Color Properties ... 24

4 RESULTS AND DISCUSSION **26**

4.1 Results 26

4.1.1 Luminescent Glasses 26

4.1.2 Blue Carbon Dots and BCDs/PVP Solution 31

4.1.3 BCDs-coated Luminescent Glasses 36

4.1.4 White Light Emission – The Comparison of TD3-3L and SD05-3L Glasses 47

4.2 Conclusion and Future Outlook 55

REFERENCES **57**

PUBLICATIONS FROM THE THESIS **66**

LIST OF SYMBOLS

T_c	Crystallization temperature
T_g	Glass transition temperature
°C	Degree Celsius
E	Energy
L_{sample}	Emission intensity from calibrated spectra by area integration
$E_{reference}$	Scattering intensity of excitation light not absorbed by reference
E_{sample}	Scattering intensity of excitation light not absorbed by sample
nm	Nanometer
λ	Wavelength
rpm	Revolutions per minute
Dy^{3+}	Dysprosium

LIST OF ABBREVIATIONS

AIQ	Aggregation Induced Quenching
BCDs	Blue Carbon Dots
CCT	Correlated Color Temperature
CIE	Commission Internationale de l'éclariage (International Commission on Illumination)
CRI	Color Rendering Index
DMF	Dimethylformamide
DSC	Differential Scanning Calorimetry
HOMO	Highest Occupied Molecular Orbit
LED	Light Emitting Diode
LUMO	Lowest Occupied Molecular Orbit
MOF	Metal Organic Framework
PEG	Polyethylene Glycol
PL	Photoluminescence
PLQY	Photoluminescence Quantum Yield
PVP	Polyvinylpyrrolidone
QCE	Quantum Confinement Effect
QD	Quantum Dots
RE	Rare Earth
SEM	Scanning Electron Microscopy
SSL	Solid State Lighting
TEM	Transmission Electron Microscopy
UV	Ultraviolet
VIS	Visible
WLED	White Light Emitting Diode
XPS	X-Ray Photoelectron Spectroscopy
XRD	X-Ray Diffraction

LIST OF FIGURES

Figure 2.1 The cross-section of a light emitting diode 5

Figure 2.2 The cross-section of WLED 6

Figure 2.3 Energy level scheme of a luminescent ion 7

Figure 2.4 The emission mechanism of fluorescence and phosphorescence 8

Figure 2.5 The photoluminescence mechanisms 9

Figure 2.6 Energy diagram of Dy^{3+} 10

Figure 2.7 The fluorescence mechanism of carbon dots 12

Figure 2.8 The quantum confinement effect of carbon dots 12

Figure 3.1 Luminescence glass synthesis 15

Figure 3.2 The macro images of samples after surface preparation 17

Figure 3.3 The schematic representation of blue carbon dot and BCDs/PVP solution synthesis 18

Figure 3.4 The macro image of synthesized BCDs/PVP solution 18

Figure 3.5 A VWR ultrasonic bath (1L) 19

Figure 3.6 SCS G3P-8 Spin Coater 19

Figure 3.7 Spin coating of BCDs/PVP solution on Dy^{3+}-doped glass 20

Figure 3.8 Philips XRD Instrument 20

Figure 3.9 Netzsch DSC Instrument 21

Figure 3.10 PG T80 + UV-Vis spectrophotometer 22

Figure 3.11 Zeiss EVO LS 10 instrument 23

Figure 3.12 Edinburgh FS5 Spectrofluorometer 24

Figure 3.13 Heated Solid Transmission Attachment 24

Figure 4.1 XRD pattern of a) tellurite and b) silicate glasses 26

Figure 4.2 DSC results of a) tellurite and b) silicate glasses 27

Figure 4.3 Absorption spectra of a) tellurite and b) silicate glasses 28

Figure 4.4 PL excitation spectra of a) tellurite and b) silicate glasses 28

Figure 4.5 PL emission spectra of a) tellurite and b) silicate glasses 29

Figure 4.6 CIE color chromaticity coordinates of a) tellurite and b) silicate glasses 30

Figure 4.7 TGA curve of BCDs/PVP solution..... 31

Figure 4.8 The absorption spectrum of BCDs/PVP solution 32

Figure 4.9 a) XPS survey spectrum and high resolution XPS spectra b) C1s, c) N1s, and d) O1s region 33

Figure 4.10 a) General bright-field TEM image b) particle size distribution histogram of BCDs 33

Figure 4.11 PL excitation spectrum of BCDs/PVP solution..... 34

Figure 4.12 PL emission spectrum of BCDs/PVP solution under 365 nm excitation ... 34

Figure 4. 13 PLQY spectrum of BCDs/PVP solution under 365 nm excitation..... 35

Figure 4.14 CIE color chromaticity diagram of BCDs/PVP solution under 365 nm excitation 35

Figure 4.15 The macro image of BCDs/PVP solution under 365 nm excitation..... 36

Figure 4.16 PL emission spectra of one-layer BCDs-coated a) TD05-1L b) TD1-L c) TD2-1L d) TD3-1L glasses under 365 nm excitation 37

Figure 4.17 CIE diagrams of one-layer BCDs-coated a) TD05-1L b) TD1-1L c) TD2-1L d) TD3-1L glasses under 365 nm excitation 38

Figure 4.18 PL emission spectra of two-layers BCDs-coated a) TD05-2L b) TD1-2L c) TD2-2L d) TD3-2L glasses under 365 nm excitation 39

Figure 4.19 CIE diagrams of two-layers BCDs-coated a) TD05-2L b) TD1-2L c) TD2-2L d) TD3-2L glasses under 365 nm excitation 40

Figure 4.20 PL emission spectra of three-layers BCDs-coated a) TD05-3L b) TD1-3L c) TD2-3L d) TD3-3L glasses under 365 nm excitation 41

Figure 4.21 CIE diagrams of three-layers BCDs-coated a) TD05-3L b) TD1-3L c) TD2-3L d) TD3-3L glasses under 365 nm excitation 42

Figure 4.22 PL emission spectra of one-layer BCDs-coated a) SD025-1L b) SD05-1L glasses under 365 nm excitation 43

Figure 4.23 CIE diagrams of one-layer BCDs-coated a) SD025-1L and b) SD05-1L glasses under 365 nm excitation 43

Figure 4.24 PL emission spectra of two-layers BCDs-coated a) SD025-2L b) SD05-2L glasses under 365 nm excitation 44

Figure 4.25 CIE diagrams of two-layers BCDs-coated a) SD025-2L and b) SD05-2L glasses under 365 nm excitation 45

Figure 4.26 PL emission spectra of three-layers BCDs-coated a) SD025-1L b) SD05-1L glasses under 365 nm excitation 46

Figure 4.27 CIE diagrams of three-layers BCDs-coated a) SD025-3L and b) SD05-3L glasses under 365 nm excitation 46

Figure 4.28 PL emission spectra of a) TD3 & TD3-3L b) SD05 & SD05-3L glasses .. 48

Figure 4.29 PL emission spectra of BCDs-coated a) TD3 and b) SD05 glasses 48

Figure 4. 30 PLQY spectra of a) TD3-3L and b) SD05-3L glasses under 365 nm excitation 49

Figure 4. 31 PL and absorbance spectra of a) TD3 and b) SD05 glasses under 365 nm excitation 50

Figure 4.32 CIE chromaticity diagrams of a) TD3 & TD3-3L and b) SD05 & SD05-3L glasses under 365 nm excitation 51

Figure 4.33 The macro images of a) TD3 & TD3-3L and b) SD05 & SD05-3L glasses under 365 nm excitation 51

Figure 4.34 The surface and cross-sectional SEM images of a-c) TD3-3L b-d) SD05-3L 53

Figure 4.35 Temperature dependent PL spectrum of a) TD3-3L b) SD05-3L glasses under 365 nm excitation 54

Figure 4.36 Heating-cooling cycles of a) TD3-3L and b) SD05-3L glasses under 365 nm excitation 54

Figure 4.37 Time dependent PLQY spectrum of a) TD3-3L and b) SD05-3L glasses . 55

LIST OF TABLES

Table 2.1 Different forms of luminescence according to the excitation source..... 7

Table 3.1 Nominal compositions of samples in tellurite and silicate glass systems..... 16

Table 4.1 PLQY values of uncoated Dy^{3+}-doped luminescent glasses..... 30

Table 4.2 Color coordinates of tellurite and silicate glasses under 365 nm excitation.. 30

Table 4. 3 Color coordinates of one-layer BCDs-coated tellurite glasses 38

Table 4. 4 Color coordinates of two-layers BCDs-coated tellurite glasses..... 40

Table 4. 5 Color coordinates of three-layers BCDs-coated tellurite glasses..... 42

Table 4. 6 Color coordinates of one-layer BCDs-coated silicate glasses 44

Table 4. 7 Color coordinates of two-layers BCDs-coated silicate glasses..... 45

Table 4. 8 Color coordinates of three-layers BCDs-coated silicate glasses..... 47

Table 4.9 Colorimetric properties of selected glasses before & after BCDs-coating 52

ABSTRACT

Development and Investigation of White Light Emitting Diodes with Blue Emitting Carbon Dots-coated Dysprosium Doped Luminescent Glasses

Beyza ÖZLEM

Department of Metallurgical and Materials Engineering

Master of Science Thesis

Supervisor: Assoc. Prof. Dr. Miray ÇELİKBİLEK ERSUNDU

In the realm of solid-state lighting applications, white light-emitting diodes (WLEDs) are highly favored as a lighting source due to their impressive luminescent properties and color quality. However, a major challenge lies in creating environmentally friendly WLEDs without compromising lighting efficiency. One promising avenue for achieving bright white light is through the use of Dy^{3+}-doped luminescent glasses, which have brought together significant interest for their ability to emit white light at an acceptable yellow-to-blue intensity ratio. However, the hypersensitivity of the Dy^{3+} at 575 nm emission band results in intense yellow emission. Therefore, using single Dy^{3+}-doped glasses to obtain white light for solid-state applications such as WLED is still a challenge. In this thesis, blue-emitting carbon dots (BCDs) are spin-coated on two series of Dy^{3+}-doped glasses that were synthesized from tellurite and silicate systems to compensate for the blue emission deficiency of Dy^{3+} by synthesizing on which to produce resin-free WLEDs. The research delves into investigating the structural, chemical, optical, and luminescence properties of uncoated glasses in order to compare tellurite and silicate glass systems following the application of BCDs-coating. Ultimately, this thesis highlights the potential of BCDs-coated luminescent glasses, showcasing their excellent luminescent properties such as bright white light emission and increased color properties.

The use of this innovative approach opens up new opportunities for the development of following generation of lighting solutions by providing an alternative material for consideration in the field of solid-state lighting applications.

Keywords: Luminescent glass, Dy^{3+}, tellurite, silicate, carbon dots, white light

ÖZET

Mavi Işıyan Karbon Kuantum Nokta Kaplanmış Disprosyum Katkılı Lüminesan Camlardan Beyaz Işık LED Geliştirilmesi ve İncelenmesi

Beyza ÖZLEM

Metalurji ve Malzeme Mühendisliği Anabilim Dalı

Yüksek Lisans Tezi

Danışman: Doç. Dr. Miray ÇELİKBİLEK ERSUNDU

Etkileyici lüminesans özellikleri ve iyi renk kaliteleri sayesinde beyaz ışık yayan diyotlar (WLED) katı hal aydınlatma uygulamalarının arasında ışık kaynağı olarak daha çok tercih edilmektedir. Bununla birlikte, aydınlatma verimliliğini düşürmeden çevre dostu WLED'ler üretmek büyük bir zorluktur. Optimum sarıdan maviye geçiş oranıyla beyaz ışık yayma potansiyellerinden dolayı Dy^{3+} katkılı lüminesan camlar, parlak beyaz ışık elde etmek için önemli derecede umut verici olup, birçok araştırmacının ilgisini çekmektedir. Ancak Dy^{3+} iyonunun 575 nm dalgaboyundaki hassasiyeti yoğun sarı ışımaya sebep olmaktadır. Bu nedenle, WLED gibi katı hal aydınlatma uygulamalarında kullanılmak üzere beyaz ışık elde etmek için sadece Dy^{3+} katkılı camların kullanılması zorluk çıkarmaktadır. Bu tezde, Dy^{3+} iyonunun mavi ışıma eksikliği giderilmek üzere mavi ışıma yapan karbon kuantum noktalar döndürmeli kaplama yöntemiyle uygulanarak reçinesiz beyaz ışık yayan diyot üretimi amaçlanmaktadır. Araştırmada, kaplanmamış camların yapısal, kimyasal, optic ve lüminesans özellikleri; mavi ışıma yapan karbon kuantum nokta kaplanmasından sonra tellürit ve silikat camların özelliklerindeki değişimin kıyaslanması için incelenmiştir. Sonuç olarak, bu tez mavi ışıma yapan karbon kuantum nokta kaplanmış lüminesan camların potansiyelini vurgulayarak, bu kaplanmış camların parlak beyaz ışık yayma ve artan renk kalitesi özellikleri gibi mükemmel

lüminesans özelliklerini ortaya çıkarmaktadır. Bu yenilikçi yaklaşımın kullanımı, katı hal aydınlatma uygulamaları alanında alternatif bir malzeme sunarak gelecek nesil aydınlatma çözümlerinin gelişimi için yeni fırsatlar yaratmaktadır.

Anahtar Kelimeler: Dy^{3+}, silikat, tellürit, karbon nokta, beyaz ışık

1
INTRODUCTION

1.1 Literature Review

Lightning accounts for a significant portion of worldwide electricity consumption and energy demand is continuously increasing with the increasing population. Therefore, the development of highly efficient lighting technologies that are environmentally friendly to reduce CO_2 emissions and have low power consumption has gained a lot of interest since it is an important demand to reduce global electricity consumption. [1, 2] WLEDs, also known as white light emitting diodes, are widely recognized as the dominant lighting technology among various alternatives, primarily due to their exceptional performance. The WLEDs are preferable due to their high luminous efficiency, longer operating life, environmentally friendly components, low power consumption and potential to decrease total energy consumption. [3, 4] Although, despite their advantageous properties, WLEDs suffer from major disadvantages, such as self-quenching, reabsorption, thermal and chemical instability, and scattering losses which need to be improved for large-scale usage.[5, 6] Hence, trivalent rare-earth (RE^{3+}) ions-doped luminescent glasses have emerged as promising color converters as an alternative for WLEDs with their excellent properties such as high optical transmittance, simple manufacturing techniques, high lanthanide solubility, and cost-effectiveness. [7-9] The rare earth ions can be doped singly or multiply into the glass host with different concentrations to tune emission properties. Additionally, the emission peaks of rare earth ions are identical in each glass system while the emission intensity changes according to the phonon energy of the host material which is another reason that different glass systems can be used as alternatives for WLEDs. Therefore, several glass systems such as tellurite [10], borate [11], silicate [12], and phosphate [13] were doped with rare earth ions to obtain white light emission. However, to obtain high quality emission, glasses should have characteristics such as low phonon energy and good lanthanide solubility. Unfortunately, some glass systems are not suitable to be used in WLED applications due to their poor mechanical and thermal properties, such as fluoride and phosphate glasses.

Among various rare earth ions, Dy^{3+} with a $4f^9$ electron configuration is one of the most preferable since it consists mainly of two bands in the blue (~484 nm) and yellow (~575 nm) regions of the visible spectrum that can directly emit white light at an appropriate yellow-to-blue intensity ratio. [14, 15] Hence, many studies have been reported on Dy^{3+} doping for white light generation in various glass systems such as, tellurite [16], silicate [17], phosphate [18], borogermanate [19], and fluorophosphate [20]. Unfortunately, the emission band of Dy^{3+} at 575 nm can be easily affected by the local environment which causes an intense yellow emission. In order to prevent this, several blue-emitting RE^{3+} ions such as Tm^{3+} are doped with Dy^{3+} to increase the blue emission intensity. However, due to the low conversion efficiency of Tm^{3+}, obtaining white light emission still remains a challenge. [21]

Lately, carbon dots (CDs) have become apromising alternative material to be utilized in the light emitting devices due to their appealing properties such as strong and wide optical absorption, tunable emission in the visible range, low toxicity, and cheap up-scale production.[22, 23] However, the progress in creating solid-state CDs capable of emitting multiple colors is hindered by the significant self-quenching observed in CDs when in the solid-state, mainly due to the aggregation-induced quenching effect (AIQ).[24] As a result of the review, an alternative strategy to obtaining white light emission with the combination of carbon dots and luminescent glasses has significant potential as a WLED. However, in order to assess the potential, through research into the optical, photoluminescence, and color properties of these material is required.

1.2 Objective of Thesis

The aim of this thesis is to synthesize a blue emitting carbon dot solution and yellow emitting Dy^{3+}-doped tellurite and silicate glasses to create a composite system that emits white light via coating and investigate their structural, optical, photoluminescence, color, and stability properties to evaluate their potential as WLEDs in solid-state lighting applications.

1.3 Hypothesis

Luminescent glass as an alternative material for WLEDs has been out in the field since these are stable hosts and various rare earth ions can be doped in multiple combinations to achieve white light emission. Among various RE^{3+} ions, the Dy^{3+} ion came forward since it has blue, yellow and red emission in it. But the blue emission is hypersensitive to

the environment and can be easily quenched. Dy^{3+} is mostly doped with Tm^{3+} in glass to increase the blue emission intensity and achieve bright white light emission. However, it remains a challenge due to the low down-conversion efficiency of Tm^{3+} which brings carbon dots forward. However, as far as our understanding goes, there has been no specific investigation dedicated to the combination of luminescent glasses with carbon dots for their potential use in WLEDs. Therefore, in this work, the combination of Dy^{3+}-doped glasses with blue-emitting carbon dots (BCDs) is proposed as an effective new strategy to compensate for the low blue light deficiency of Dy^{3+} ions. Hence, two series of Dy^{3+}-doped glasses are synthesized from different glass systems, i.e., tellurite and silicate, and spin-coated with BCDs. Accordingly, the chemical, structural, optical, and photoluminescence (PL) properties of BCD-coated Dy^{3+}-doped tellurite and silicate glasses are investigated in detail.

2
THEORETICAL INFORMATION

2.1 Energy and Solid-State Lighting Technologies

Energy, which is in a term of basically an ability to do work, is a key factor for the life occurs in the entire universe. Energy is essential but especially the electricity. Despite the fact that it is a basic human need but foremost electricity is essential to continuing living both at day and at night. Electricity helps us to do daily tasks such as powering devices that make daily living more efficient, living under the dark and simply refrigerating the food etc. Nowadays, energy consumption of the world is getting more attention since the population of the world increases while throughput decreases over time which makes human worry about the future.[25, 26] In specific, almost 20% of consumed energy of the world accounts for the residential buildings and more than 22% of global energy consumption in each building is for electricity that is also responsible for the 17% of greenhouse gas emissions which is an example of environmental issues that keeps on rising.[27] In the past, people used many lighting sources which improved over time since we humans would always open a space for improvement. It started with natural light then candles which led to the usage of gas lamps that will later mirror the advancement of hydrocarbon fuel production. But incandescent light bulb came forward after Edison discovered carbonized bamboo filament can burn 1000 hours invention which was a milestone in the industry. The incandescent lights were dominant in the industry until fluorescent lights came forward. Unfortunately, the efficiency of these lighting sources is limited by both temperature and the energy loss. In contrast, solid state lighting energy technologies is not limited by these and also, have long lifetime and low energy consumption. Since energy used for lighting technologies all around the world, which contributes a fair percentage of the planet's greenhouse gases, will be always increasing since artificial light with reduced energy usage is important for human's daily life, solid state lighting technologies became the most efficient lighting source in present. [28, 29]

Solid state lighting describes how the light is obtained, especially includes the mechanism of light emitting diode (LED). The LED is basically a device that is in the solid state and produces light via electric energy. There are three layers in LED as n-type semiconductor,

p- type semiconductor and depletion layer which separates the n- and p- layers (see Figure 2.1). When an electric current passes through the LED, electrons in the semiconductor recombine with electron holes which at the end releases energy in the form of photons. As a result, a semiconductor device, the diode which energized by electricity, emits light and can glow in various colors depending on the ingredients. [30, 31]

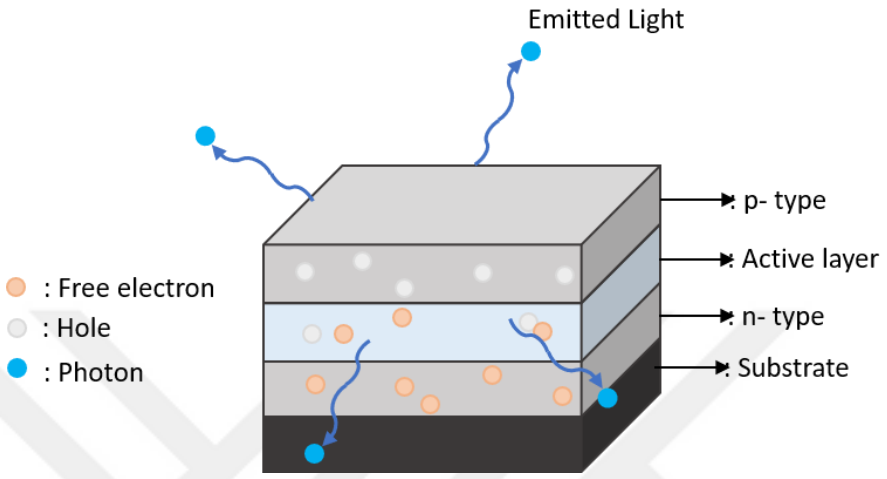


Figure 2.1 The cross-section of a light emitting diode

Even though LEDs are similar to incandescent bulbs only fundamentally, there are several differences such as lifetime, color properties or environmentally side. LEDs can last up to 50 times longer than other lighting technologies.[32] Also, LEDs are environmentally friendly since there is no safety concerns such as broken glass in incandescent bulbs. Additionally, the color diversity of LEDs which can be improved with the combination of multiple options, makes them suitable for every condition. But most significant one is the source which effects all other properties. The filaments in incandescent bulbs burns by electricity and produces heat and light. However, filament eventually decays. On the other hand, in solid state lighting the electrons inside diode realigns and diode remains unchanged. [33]

Throughout the years, significant advancements have been made in the development of highly efficient red, orange, and yellow LEDs, establishing them as efficient lighting devices. However, WLEDs differ from the traditional LEDs with their long lifetime, high brightness, and their ability to emit polychromatic light. There are two common ways to obtain white light in LEDs. WLEDs were initially introduced by utilizing three LED chips that emit the primary colors of red, green, and blue, in order to achieve the production of white light. But this system required four individual lead electrodes for each chip. So, an

alternative method was employed, relying on the utilization of a UV LED chip and a phosphor that assimilates UV light and transforms it into white light.[34] Conventional WLEDs consists of four parts as illustrated in Figure 2.2: a blue LED chip that emits blue light, yellow phosphor that emits yellow light after excitation, epoxy resin that holds blue LED chip and yellow phosphor together and silicon lens that accumulates obtained white light through. When current is applied through blue LED chip, the generated blue photons excite yellow phosphor layer which emits yellow light and the combination of these blue and yellow light yields white light.

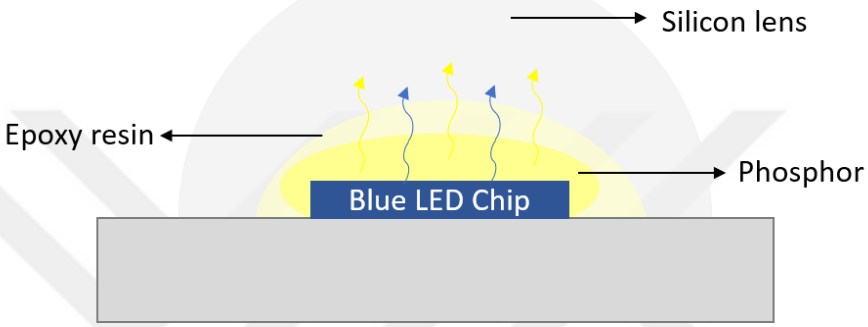


Figure 2.2 The cross-section of WLED

WLEDs are the fundamental component of solid-state lighting technologies since WLEDs also have the outstanding features such as long lifetime and high light power as LEDs. However, not only LEDs but WLEDs have some weaknesses that need improvements. The epoxy resin used in conventional WLEDs is a form of polymer which is degradable. Since there is heat output as a result of electricity, the whole system becomes thermally and chemically unstable. Additionally, the refractive index difference between epoxy resin and phosphor causes scattering losses and low optical transmittance of phosphor leads to decrease in light efficiency. To overcome these obstacles, developing environmentally friendly and energy-sufficient lighting sources became important and many studies have been focused on this matter. Notwithstanding, one of the most sufficient ways to obtain white light with features as sustainable, easy to fabricate and cheap, is to use glass matrix as a host for rare earth elements (RE).[3, 35, 36]

2.2 Luminescence

When an atom's electrons are in their steady state, they can be stimulated to move to higher energy levels by absorbing a photon. The energy required for an electron to transition to a higher level varies depending on the atom and its electrons. Eventually,

electrons will return to their ground state as they are unable to remain in their excited state for an extended period of time. When an electron transitions from its excited state to its ground state, it releases energy in the form of light and that energy is equal to the difference between the energies of the steady and excited state. Luminescence is a general phenomenon where an energy source excites an atom out of its ground state to a higher energy state which is called the excited state, and then the electron returns to its ground state whilst releasing subsequent emission of photons or energy in the form of a radiative or non-radiative transition that is illustrated in Figure 2.3. However, the emission obtained from luminescence is not a thermal radiation, nor does it include the emission of blackbody radiation since material emits light without being heated up.[37, 38]

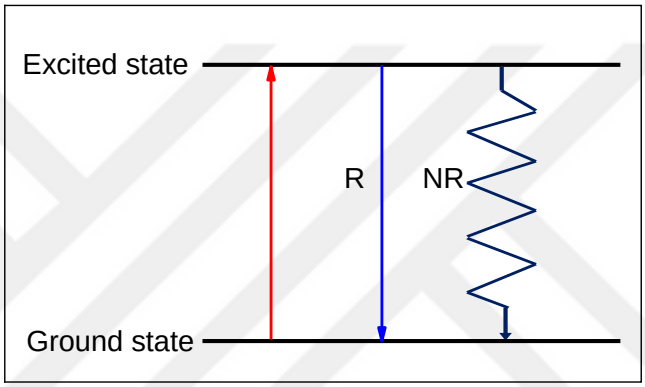


Figure 2.3 Energy level scheme of a luminescent ion

A large number of both organic and inorganic substances show luminescent characteristics, and there are several types of luminescence, each depends on the excitation source or trigger of the energy, such as bioluminescence, electroluminescence, photoluminescence, etc., as stated in Table 2.1.[39-42]

Table 2.1 Different forms of luminescence according to the excitation source

Luminescence Type	Excitation Source	Example of Application
Bioluminescence	Biochemical Reaction	Jellyfish
Chemiluminescence	Chemical Reaction	Emergency Signals
Cathodoluminescence	Electrons	Monitors
Mechanoluminescence	Mechanical Energy	Crack Detection
Photoluminescence	Photons	Fluorescent Lamps

In the process of photoluminescence, the absorbed energy is re-emitted as light, which can be visible, ultraviolet, infrared, etc., and the wavelength of the light is characteristic of the luminescent material. After the absorption of the radiation, the emission of light takes place at a characteristic time, which sub-classifies luminescence according to the duration of emission, which are fluorescence and phosphorescence, as illustrated in Figure 2.4. [43, 44] Fluorescence is a spontaneous and temperature independent process that can occur simultaneously with the absorption of radiation and then stop after the radiation ceases. On the removal of the excitation source, an exponential afterglow can be observed with a lifetime less than 10^{-8} seconds. However, phosphorescence is a temperature dependent process that can continue for more than 10^{-8} seconds even after the removal of the excitation source. The reason phosphorescence takes longer is because there is an intermediate level called the metastable level between the excited and ground states, which forbids the transitions from level to level and is appertaining to the delay between the radiation absorption and time to reach full intensity.[45, 46]

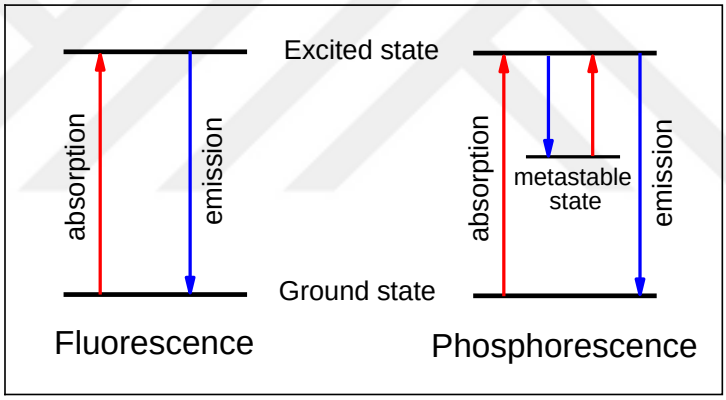


Figure 2.4 The emission mechanism of fluorescence and phosphorescence

The mechanisms of photoluminescence are divided into three categories: down-shifting (DS), down-conversion, which is also called quantum cutting (QC), and up-conversion (UC) (see Figure 2.5). The down-shifting and down-conversion processes are very similar, and both are considered Stokes processes. In the down-shifting, for each absorbed high energy photon, the maximum amount of one photon lower in energy occurs. Nevertheless, in down-conversion, the absorbed photon is converted into two or more photons with lower energies, which results in higher quantum values. On the contrary, up-conversion refers to a non-linear phenomenon known as anti-Stokes conversion, where one or more photons with lower energy are assimilated and subsequently transformed into photons of higher energy.[47, 48]

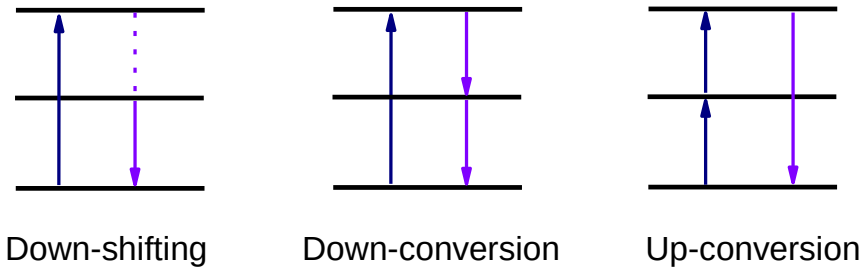


Figure 2.5 The photoluminescence mechanisms

2.2.1 Photoluminescent Materials

Photoluminescent materials, which have the ability to absorb energy and then emit that energy as photons of light, come in different structures, such as amorphous and crystalline or organic and inorganic, and can have varying luminescent behaviors. Most luminescent materials have relatively low quantum efficiencies due to non-radiative transitions such as inter-system crossings and vibrational transitions that compete with radiative transitions. Unlikely, organic compounds that contain strong fluorescent molecules such as fluorescein, eosin, rhodamine, and stilbene exhibit almost 100% quantum efficiencies, and they are mostly used as organic brighteners for invisible markers since they can only be excited by invisible ultraviolet radiation, also called black light. [49, 50] Among photoluminescent materials, metal-organic frameworks (MOFs) are hybrid materials formed as a combination of metal ions or clusters and organic bridging ligands via coordination linkages. MOFs have diversity and flexibility to be synthesized since there is a combination of organic and inorganic components together. [51, 52] Another photoluminescent materials are quantum dots (QDs) which are semiconductor crystal materials in nano dimensions, exhibit a wide range of quantum efficiencies, but generally show quantum efficiencies of 50% and above. Carbon dots as an example of quantum dots are organic materials that can be easily synthesized and emit in the visible spectrum. [54] Additionally, the transition metals display photoluminescent characteristics and have relatively lower quantum efficiency. In materials doped with transition metals, luminescence occurs between d-d electronic transitions, which depend on the host lattice due to the strong electron phonon coupling since transition metal ions have an incompletely filled d-shell which that is not shielded from the host lattice. [55-57] Furthermore, the rare-earth ions (lanthanides) have unique electron configurations (4f) and numerous energy levels, which endow luminescent characteristics such as broad

optical absorption, tunable emission, and a long lifetime. [58] For lanthanides, the total quantum efficiency varies depending on the nature of the lanthanide ions. In recent years, rare-earth ion doped glasses came forward and displayed excellent luminescent properties that are used in several applications such as solar cells, LEDs, anti-counterfeiting. [59, 60] Particularly, lanthanide-doped materials that display a down-conversion mechanism showed promising results when used in WLED applications. [9, 61-64]

2.2.2 Down-Conversion Mechanism of Dy^{3+}

The down conversion mechanism, as one of the three main photoluminescence mechanism, of Dy^{3+} also occurs as the same as other lanthanides.[5] The one photon with high energy is absorbed and excited from ground state to excited state and, converted into two or more low energy photons. This process is called down-conversion since the quantum values are larger than obtained. Also, the process of down-conversion is commonly referred to as the Stokes process, as it follows Stokes' rule, which dictates that the wavelength of luminescence is greater than the wavelength of the incident radiation.[65] Among other lanthanide ions, trivalent Dy^{3+} with $4f^9$ electron configuration is considered as the most suitable ion to be used in white light emission studies considering the emissions of Dy^{3+} in blue, yellow, and red region in the spectrum which is illustrated in Figure 2.6.[66, 67]

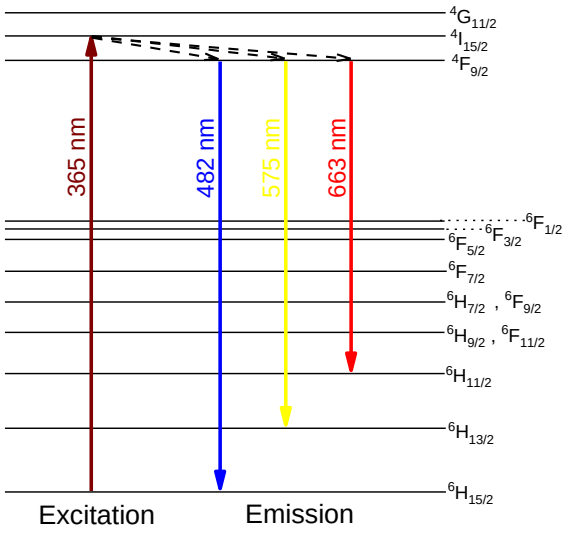


Figure 2.6 Energy diagram of Dy^{3+}

The $^4F_{9/2} \rightarrow {}^6H_{15/2}$ transition located in 482 nm is insensitive. However, the $^4F_{9/2} \rightarrow {}^6H_{13/2}$ transition that located in 575 nm is hypersensitive and easily affected by the phonon

energy of host material and environment due to the selection rule ($\Delta L = \pm 2$ and $\Delta J = \pm 2$). [68] Considering the luminescence properties of Dy^{3+} ion depends on the environment, several studies have been reported to use Dy^{3+} in order to obtain white light emission and, specifically in WLEDs. [69-72] Most of these studies included doping Dy^{3+} in several different glass host since glass systems have favorable properties such as high thermal and chemical stability. However, single Dy^{3+}-doped glasses have low quality white light emission due to the yellow-to-blue (Y/B) intensity ratio. In order to increase the blue emission intensity of Dy^{3+}, other lanthanides such as Tm^{3+} is also doped in glasses but the low down-conversion emission efficiency of Tm^{3+} still resulted in low photoluminescent characteristics.[73, 74] Therefore, choosing appropriate luminescent material to combine with Dy^{3+} is a key factor to obtain white light emission for solid-state lighting applications such as WLED.

2.2.3 Fluorescence Mechanism of Carbon Dots

Recently, besides lanthanide-doped glasses, also fluorescent carbon dots have gained a lot attention as promising luminescent material for lighting applications due to their excellent properties such as tunable photoluminescence, wide optical absorption, high-water solubility, and low toxicity.[75, 76] Carbon dots are carbon-based nanomaterials that consists a spherical-like core with the stack of multiple graphene and functional groups on the surface.[77] Generally, top-down and bottom-up synthesis are the two distinct methods used to create fluorescent carbon dots. The top-down technique essentially reduces large-sized precursors of carbon, like graphite, graphene oxide, and carbon nanotubes, into smaller CDs. Physical or chemical methods like laser ablation and electrochemical oxidation are commonly in top-down approaches. [78, 79] On the other hand, bottom-up approaches focus on the creation of larger CDs from smaller ones. Combustion methods, such as microwave synthesis, chemical oxidation, and solvothermal treatments, are utilized in bottom-up approaches to synthesize CDs from molecular precursors. [80, 81] However, even though bottom-up approaches are simple processes, the quantum efficiency of particles are low since obtained structures are very amorphous.[82]

The fluorescence mechanism of CDs mostly depended on the interaction between the core and the chemical groups that surrounds the core.[83] When valance band of CDs separates from conduction band, the electrons in conduction band moves to an empty state (see

Figure 2.7). Also, the direct combination of electrons and holes gets enabled and results in band gap fluorescence which produced by the radiation transition of the electron-hole pairs in the sp2. CDs with large conjugated π-domains and a few functional groups on the surface results in fluorescent center in CDs which is a consequence of the quantum confinement effect (QCE). [84]

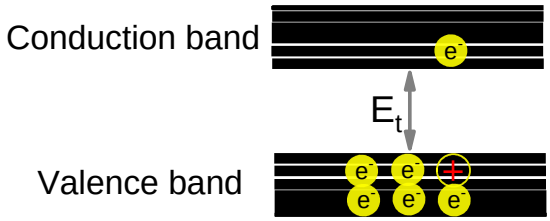


Figure 2.7 The fluorescence mechanism of carbon dots

The QCE is a simply size effect where size refers to sp2 domain than the particle size and as the size decreases to the nanoscale, quasi-continuous electronic levels transform into discrete energy level. The smaller size of CDs conjugated π-domain results in less delocalization and a larger energy difference between the highest occupied molecular orbital (HOMO) and the lowest unoccupied molecular orbital (LUMO), known as the band gap. Therefore, the emission peak of CDs shifts to the blue region (see Figure 2.8).[85]

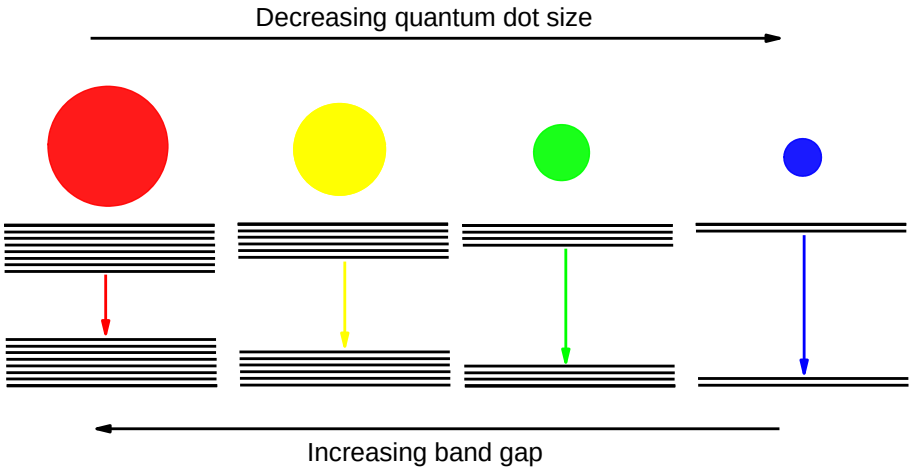


Figure 2.8 The quantum confinement effect of carbon dots

Consequently, the luminescent properties of CDs can be tuned with the band gap adjustment by regulating the size of the conjugated π-domains which depends on the chemical structure of CDs. [86] However, the fluorescent emission of CDs is limited due to the luminescence band with the full-width at half-maximum is higher than 80 nm. As a result, low color purity characteristics are obtained when carbon dots are used in lighting applications.[87] Additionally, when CDs aggregate, the non-luminescent symmetrical molecules occurs due to the aggregation-induced quenching (AIQ) effect. [88] Due to the AIQ, CDs promotes substantial self-quenching as it aggregates in solid-state and the emission decreases compared to the solution state.[24, 89] Although CDs have great luminescent properties, alternative approaches must be introduced for the effective use of CDs in solid-state applications.

2.2.4 White Light Emission from Down-Conversion

Up until now, many studies and research have been reported for the white light emission via down-conversion. In particular Wang et al, calculated color coordinates for SiO-MgO-B_2O_3 glasses in the range of x=0.27-0.35, y=0.22-0.34 with varying Dy^{3+} concentration. [90] Mariselvam et al. investigated the luminescent characteristics of Dy^{3+}-doped niobium fluoro borotellurite glasses under 453 nm excitation, calculated color coordinates as x=0.38, y=0.42 and discussed their potential to be used as WLEDs. [69] Vijayalakshmi et al. synthesized Dy^{3+}-doped lithium zinc borate glasses for WLED applications and calculated color coordinates as x=0.39, y=0.42 with the 3886 K CCT value under 362 nm excitation. [91] Furthermore, Fang et al. studied the luminescence behavior of carbon dots under several excitation wavelengths and found out that under 365 nm excitation, hydrothermal synthesized carbon dots display strong blue emission but also stated further investigation is required due to the fact that solution-based carbon dots have poor stability. [92] An et al. synthesized multicolor solid fluorescent carbon dots in order to mix them for WLED applications, but observed a significant decrement in the fluorescence quantum efficiency and lifetime of the solid blue emitting carbon dots compared to those of the solution ones, which indicates the quenching behavior caused by the π - π interaction. [93] Consequently, in the research of an alternative material for WLED applications, there is no study yet focused on the combination of inorganic and organic materials, such as luminescent glasses and carbon dots. While previous studies have predominantly focused on single-material systems, this thesis proposes a novel approach by integrating Dy^{3+}-doped tellurite and silicate glasses as yellow emitting sources, and carbon dots dispersed in a polyvinylpyrrolidone (PVP) solution as blue emitting sources. The specific combination of yellow-emitting Dy^{3+}-doped tellurite and silicate glasses with blue-emitting carbon dots dispersed in a PVP solution offers the potential for achieving a balanced and high-quality white light output. The objective is to achieve white light

emission by harnessing the complementary emission characteristics of these materials. The evaluation of this alternative material for WLEDs with white light emission involves several aspects such as the spectral characteristics of the emitted light, including color temperature, color rendering index (CRI), and correlated color temperature (CCT). Additionally, the efficiency and stability of the material system need to be assessed such as thermal management, and operational lifetime. In conclusion, the combination of Dy^{3+}-doped tellurite and silicate glasses as yellow emitting sources, along with carbon dots dispersed in a PVP solution as blue emitting sources, presents a promising alternative material for WLED applications. By harnessing the complementary emission characteristics of these inorganic and organic materials, it is possible to achieve white light emission with improved color quality and efficiency. Further research and development are necessary to fully explore the potential of this material combination and enable its practical implementation in future WLED technologies.

3
EXPERIMENTAL STUDIES

3.1 Sample Synthesis

In order to obtain white light that to be used in the investigation of white LEDs, among other rare earth elements Dy^{3+} ion, due to its multi-emissive behavior that includes blue, yellow and, even though it is small, red emission; was added to the tellurite and silicate glass systems. When compared to the other glass systems, tellurite glasses have shown good lanthanide solubility and silicate glasses have good chemical and thermal stability as a host material. However, in order to achieve white light emission, the blue emission deficiency of Dy^{3+} was supported with another luminescent source which was chosen as carbon dots that emits blue light and has been applied on the surface of luminescent glasses.

3.1.1 Luminescent Glass Synthesis

For the purpose of obtaining white light emission, various glasses with different Dy^{3+} ion concentrations were synthesized. Therefore, two distinct sets of Dy^{3+}-doped samples in tellurite and silicate glass systems were prepared in addition to comparing the luminescent behaviors. $25Li_2O–25WO_3–(50\text{-}x)\ TeO_2–xDy_2O_3$ (x = 0.5, 1, 2, 3, 4 mol %) with molar composition, five different tellurite glass samples were synthesized as a first set. $15Na_2O–20CaO–15B_2O_3–5Al_2O_3–(45\text{-}x)\ SiO_2–xDy_2O_3$ (x = 0.25, 0.5, 1 mol %) with molar composition, three different silicate glass samples were synthesized as second set. Both of the glass samples were synthesized using the traditional melt-quenching technique as shown in Figure 3.1.

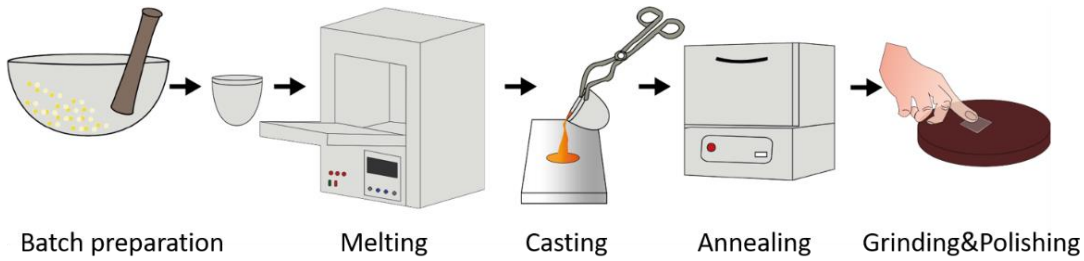


Figure 3.1 Luminescence glass synthesis

The prepared glass samples were labeled according to their Dy^{3+} concentrations as TD*x* and SD*x* (*x* represents mol% of Dy^{3+}). A detailed overview of the chemical composition of samples along with their codes is given in Table 3.1.

Table 3.1 Nominal compositions of samples in tellurite and silicate glass systems

Glass System	Sample Code	Nominal Composition (mol %)								
		Li_2O	WO_3	TeO_2	Na_2O	CaO	B_2O_3	Al_2O_3	SiO_2	Dy_2O_3
Tellurite	TD05	25	25	49.5	-	-	-	-	-	0.5
	TD1	25	25	49	-	-	-	-	-	1
	TD2	25	25	48	-	-	-	-	-	2
	TD3	25	25	47	-	-	-	-	-	3
	TD4	25	25	46	-	-	-	-	-	4
Silicate	SD025	-	-	-	15	20	15	5	44.75	0.25
	SD05	-	-	-	15	20	15	5	44.5	0.5
	SD1	-	-	-	15	20	15	5	44	1

Samples were synthesized using high purity chemicals of Li_2O (99%), WO_3 (99.9%), TeO_2 (99.99%), Na_2O (99.5%), CaO (99.5%), B_2O_3 (99.5%), Al_2O_3 (99%), SiO_2 (99.5%) and Dy_2O_3 (99.99%) from Sigma-Aldrich and Alfa Aesar. Starting chemicals were weighed using a Precisa/XB 220A high precision scale (10^{-4} g) and thoroughly mixed for 10-15 minutes in an agate mortar with a pestle in order to ensure complete homogeneity of glass batch. Thereafter, 10 grams of each well mixed tellurite and silicate batches were placed into platinum crucibles and melted at 800 °C and 1150 °C for 30 min and 75 min, respectively, under atmospheric condtions.

The obtained melts were poured into pre-heated stainless-steel molds and pressed with another steel plate to obtain as-cast samples. In order to eliminate residual internal stress originating from rapid cooling of samples during melt quenching, the glass samples were annealed in a preheated furnace below the glass transition temperature of each glass system at 310 °C for 3 hours and 450 °C for 5 hours for glass samples, respectively, and cooled to room temperature inside the furnace. Techniques and conditions used for glass synthesizing were kept constant for all samples studied in this thesis.

In order to have homogeneous coating on the glass surface and to investigate morphological and luminescent properties, all samples must have clean, plan-parallel, and scratch-free surfaces. Therefore, all samples were ground using different sizes of

sandpaper (120, 320, 800, 1200, and 2500) and polished with 1μ polishing pad using diamond paste with a size of 1μ. The images of samples after surface preparation are shown in Figure 3.2.

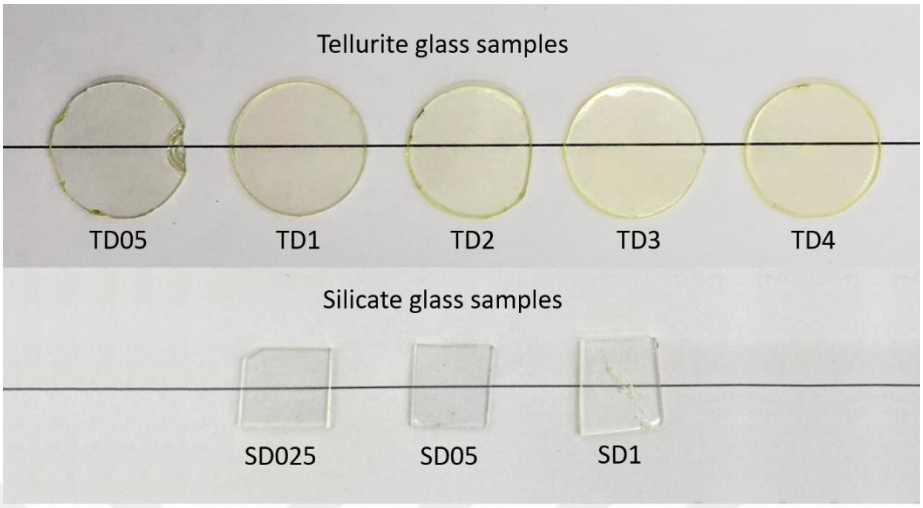


Figure 3.2 The macro images of samples after surface preparation

3.1.2 Blue Carbon Dots and BCDs/PVP Solution Synthesis

The BCDs were prepared with a facile thermal method using carob molasses as a natural carbon source, which was obtained from a local supermarket, polyethylene glycol (PEG) as a passivation agent, and urea as a nitrogen source. The PEG and urea were purchased from Sigma-Aldrich. As a first step to prepare BCDs, 1.0 g of carob molasses was diluted in deionized water with a 1:10 (w/v) ratio and labeled as *Solution 1*. PEG and urea (1:8:4 w/w) were mixed and dispersed in 2 mL of a 1:1 v/v) water/ethanol solution at the same time and labeled as *Solution 2*. Then *Solution 1* and *Solution 2* were combined and heated in a Teflon oven vessel at a temperature of 250 °C for a duration of 45 minutes, resulting in brown material. The brown material obtained was combined with 6 mL of deionized water and subjected to centrifugation at a speed of 13500 rpm for a duration of 20 minutes, ensuring the absence of any significant particles. Following the centrifugation process, the uniform supernatant was then dried overnight at a temperature of 90 °C under a vacuum environment and, as a result, BCDs were successfully obtained.

To prepare BCDs/PVP solution, 1.5 g of poly vinylpyrrolidone (PVP) and dimethylformamide (DMF) were mixed and dissolved for 15 minutes in a magnetic stirrer. 15 mg of BCDs were added into obtained solution and sonicated for 5 minutes.

After sonication 15 minutes of additional magnetic stirring were applied. Figure 3.3 shows a schematic representation of how to prepare BCDs and BCDs/PVP solution.

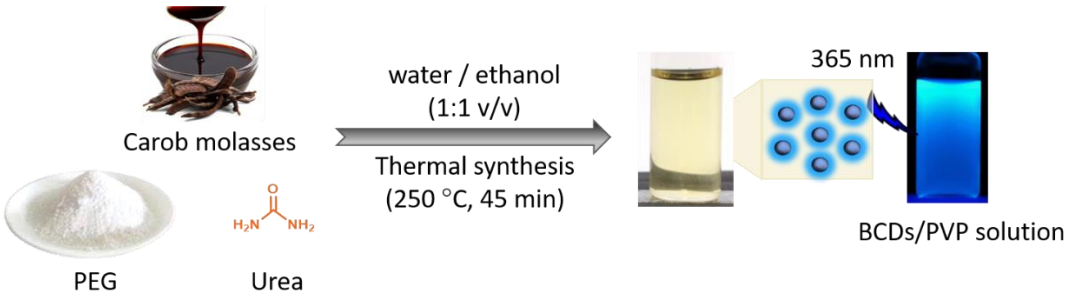


Figure 3.3 The schematic representation of blue carbon dot and BCDs/PVP solution synthesis

The obtained homogeneous BCDs/PVP solution was presented in Figure 3.4 under daylight.



Figure 3.4 The macro image of synthesized BCDs/PVP solution

3.1.3 The Coating Process

After surface preparation, the glass samples of both tellurite and silicate glass systems were cleaned in an VWR Ultrasonic Bath (see Figure 3.5) for 15 minutes to remove any excess residue using acetone, distilled water, and ethanol consecutively.



Figure 3.5 A VWR ultrasonic bath (1L)

20 µL of BCDs/PVP solution was spin-coated on glass samples at SCS G3P-8 Spin Coater (see Figure 3.6). The spin coating process was done at 3000 rpm for 30 seconds for each glass and, BCDs-coated glasses were obtained.



Figure 3.6 SCS G3P-8 Spin Coater

Following that, BCDs-coated glasses were subjected to a drying process at a temperature of 120 °C for a duration of 1 hour. This process was taken to eliminate any excess solvent and achieve a coating on the glass surface that is environmentally stable. The coating

process, which was demonstrated in Figure 3.7, was repeated until three layers of BCDs coating were obtained on glasses. Additionally, BCDs-coated glasses were labeled according to the number of coating layers applied, i.e., TD3–3L and SD05–3L.

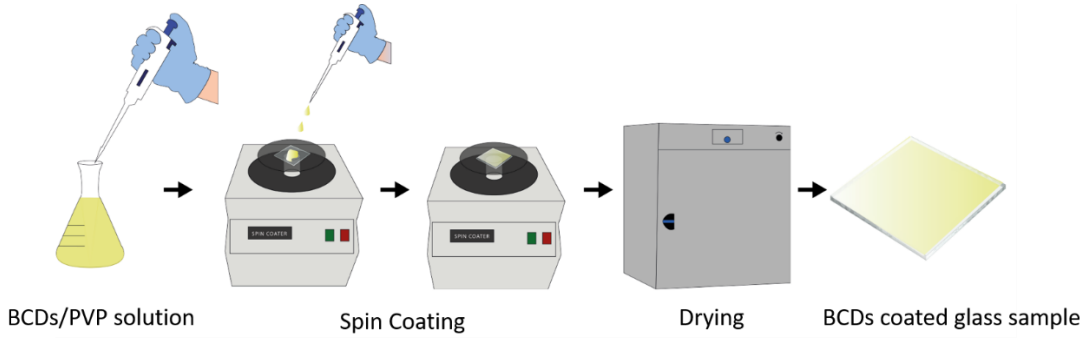


Figure 3.7 Spin coating of BCDs/PVP solution on Dy^{3+}-doped glass

3.2 Sample Characterization

3.2.1 Structural Analysis

The Philips PANanalytical X'pert Pro XRD instrument (shown in Figure 3.8) is employed to observe and verify the non-crystalline properties of tellurite and silicate glass samples. The examination is conducted with CuKα radiation at 45kV and 40 mA, employing a 0.02° step size interval within the 2θ range spanning from 20°-80°.



Figure 3.8 Philips XRD Instrument

3.2.2 Thermal Analysis

Differential scanning calorimetry (DSC) analysis is carried out to determine the glass transition temperatures (T*g*) and crystallization onset temperatures (Tc) of Dy^{3+}-doped tellurite and silicate glasses in a Netzsch DSC 204F1 instrument as shown in Figure 3.9. The DSC instrument has a sensitivity limit of < 0.1 μV and an error estimate of ± 1 °C. The analysis involves using a constant sample weight of 25 mg (± 1 mg) placed in aluminum pans. The samples are then subjected to heating up to 520 °C at a rate of 10 °C/min under a flowing argon gas atmosphere of 25 mL/min.



Figure 3.9 Netzsch DSC Instrument

The thermal stability of synthesized BCDs/PVP solution is confirmed using a Mettler Toledo Thermal Analysis System TGA/DSC 3+ with a heating rate of 10 K/min from 25° to 800°C under a nitrogen atmosphere at a flow rate of 40 mL/min.

3.2.3 Optical Analysis

The optical absorption spectra of BCDs/PVP solution and sample glasses are measured using a PG T80 + UV-Vis spectrophotometer as shown in Figure 3.10. All measurements are performed at room temperature with 0.1 nm resolution and, between the wavelength ranges of 300 and 1000 nm.



Figure 3.10 PG T80 + UV-Vis spectrophotometer

3.2.4 Chemical Analysis

The Specs-Flex XPS system is employed for utilizing X-ray Photoelectron Spectroscopy (XPS) to analyze the surface functionalization and chemical composition of BCDs.

3.2.5 Morphological Analysis

The morphology and particle size of BCDs are characterized by Transmission Electron Microscopy (TEM) using a JEOL USA JEM-1400 instrument. Using the ImageJ program, the average particle size and standard deviation are determined by measuring the diameter of a minimum of 100 particles.

Scanning electron microscopy (SEM) imaging is used for morphology analysis of BCDs-coated glasses by coating the sample surface with Au/Pd on a Zeiss EVO LS 10 instrument (see Figure 3.11) operating at 5 kV, Additionally, cross-sectional SEM micrographs are used to determine the thickness of coatings.

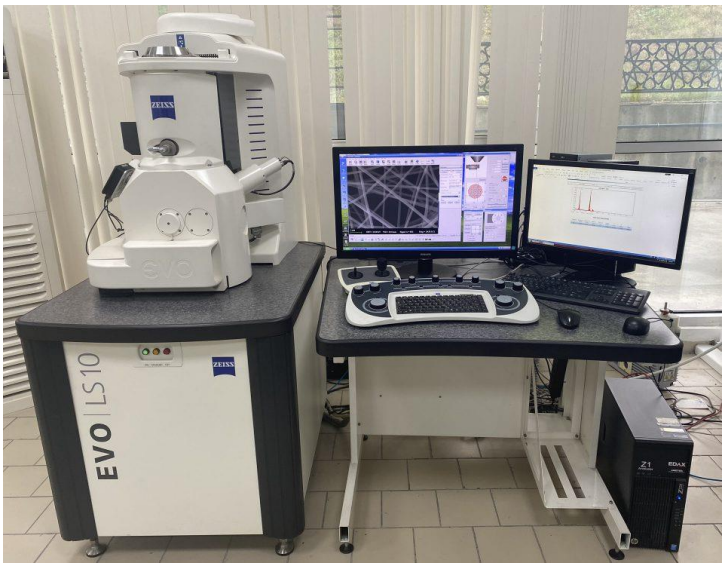


Figure 3.11 Zeiss EVO LS 10 instrument

3.2.6 Photoluminescent Analysis

The PL excitation and down-conversion PL emission spectra of BCDs/PVP solution, Dy^{3+}-doped tellurite and silicate glasses and, BCDs-coated glasses are measured in an Edinburgh Instruments FS5 spectrofluorometer (see Figure 3.12) using a 150 W xenon lamp as an excitation source with high spectral resolution (signal to noise ratio of water Raman signal > 6000:1). Also, absolute PL quantum yield (PLQY) values are measured in the Edinburgh Instruments FS5 spectrofluorometer by using an integrating sphere (150 mm internal spherical cavity, polytetrafluoroethylene coated) under 365 nm excitation wavelength. The PLQY values of BCDs/PVP solution, Dy^{3+}-doped glasses and BCDs-coated glasses are characterized with an estimated error rate of ± 5 % with the following equation:

$$PLQY = \frac{number\ of\ emitted\ photons}{number\ of\ absorbed\ photons} = \frac{L_{sample}}{E_{reference} - E_{sample}} \quad (3.1)$$

where L_{sample} corresponds to the emission intensity obtained by integrating the area under calibrated emission spectra, $E_{reference}$ and E_{sample} represent the scattering intensities of excitation light that are not absorbed by the reference and sample, respectively. For each sample, the PLQY measurements were repeated ten times and the average values were chosen to ensure data reliability.

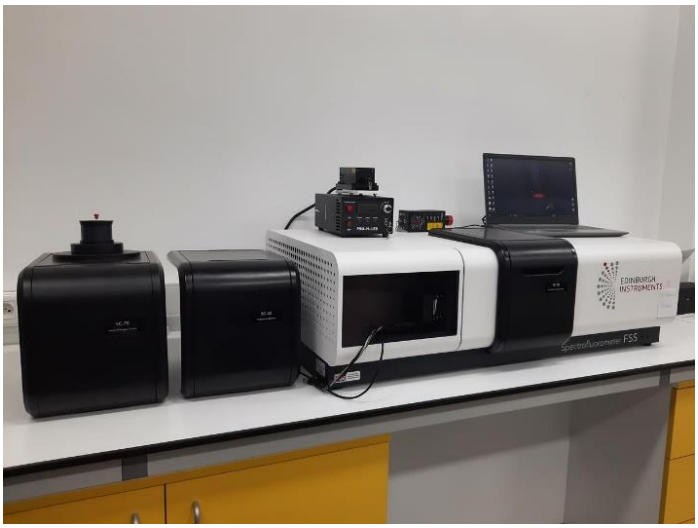


Figure 3.12 Edinburgh FS5 Spectrofluorometer

Each BCDs-coated glass was placed into a Pike Technologies heated solid transmission attachment (see Figure 3.13) which was connected to the spectrofluorometer. Temperature-dependent photoluminescence (PL) measurements are conducted by incrementally raising the temperature from 30 °C to 120 °C, followed by cooling back down to 30 °C. This process is repeated up to five heating-cooling cycles, during which the PL data is recorded.



Figure 3.13 Heated Solid Transmission Attachment

3.2.7 Color Properties

The colorimetric properties of the samples, including Commission internationale de l′éclairage (CIE) 1931 color coordinates, color rendering index (CRI), correlated color temperature (CCT), and color purity values, are determined using the OSRAM Color Calculator software based on the PL emission spectra.

The data from the down-conversion PL emission spectra is used in order to determine the chromaticity coordinates of samples by means of following equations:

$$x = X/(X + Y + Z) \quad (3.\ 2)$$

$$y = Y/(X + Y + Z) \quad (3.\ 3)$$

$$z = Z/(X + Y + Z) \quad (3.\ 4)$$

The three tristimulus values X, Y and Z represents the three main colors of red, green, and blue, respectively and can be determined using equations given below:

$$X = \int_{400}^{700} P(\lambda)\bar{x}(\lambda)\, d\lambda \quad (3.5)$$

$$Y = \int_{400}^{700} P(\lambda)\bar{y}(\lambda)\, d\lambda \quad (3.\ 6)$$

$$Z = \int_{400}^{700} P(\lambda)\bar{z}(\lambda)\, d\lambda \quad (3.\ 7)$$

where the variable λ represents the wavelength of monochromatic color of light, $P(\lambda)$ denotes the spectral power distribution and x, y and z refer to the color-matching functions.

McCamy's formula is utilized to calculate the correlated color temperature (CCT) of the samples:

$$CCT = -449n^3 + 3525n^2 - 6823n + 5520.3 \quad (3.\ 8)$$

where

$$n = \frac{X - X_e}{Y - Y_e} \quad (3.\ 9)$$

and $X_e = 0.332$ and $Y_e = 0.186$ are values for chromaticity epicenter.

Color rendering index (CRI) values of samples are determined using Color Calculator application developed by German lighting manufacturer OSRAM.

Color purity values of samples are obtained using the following equation:

$$Color\ purity\ (\%) = \frac{\sqrt{(x - x_{ee})^2 + (y - y_{ee})^2}}{\sqrt{(x_d - x_{ee})^2 + (y_d - y_{ee})^2}} \quad (3.\ 10)$$

where (x, y) is the CIE color coordinates of samples, while (x_d, y_d) and (x_{ee}, y_{ee}) represent the dominant wavelength and equal energy point, respectively.

4
RESULTS AND DISCUSSION

4.1 Results

The outcomes of all characterizations, including structural, thermal, optical, chemical, morphological, and photoluminescence examinations, as well as color characteristics and CIE color coordinates for samples, are provided in detail in this section.

4.1.1 Luminescent Glasses

The amorphous nature of synthesized luminescent tellurite and silicate glasses were confirmed with the XRD graphs shown in Figure 4.1a and Figure 4.1b. It can be seen from the figures that there are no crystalline peaks except a broad hump between 25˚-35˚ which indicates amorphous glasses were obtained.

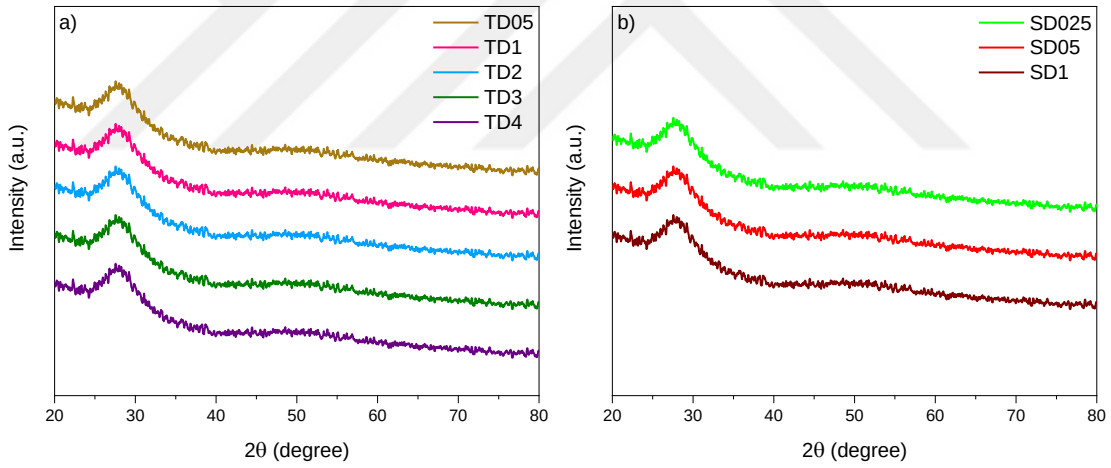


Figure 4.1 XRD pattern of a) tellurite and b) silicate glasses

Differential scanning colorimetry analysis was conducted to measure the thermal properties of both tellurite and silicate glasses, and the thermograms are given in Figure 4.2. As a result of thermal analysis, the glass transition temperature (T_g) was obtained as 327, 329, 334, 337 and 343 °C for TD05, TD1, TD2, TD3 and TD4, respectively and 541, 544 and 547°C for SD025, SD05 and SD1, respectively.

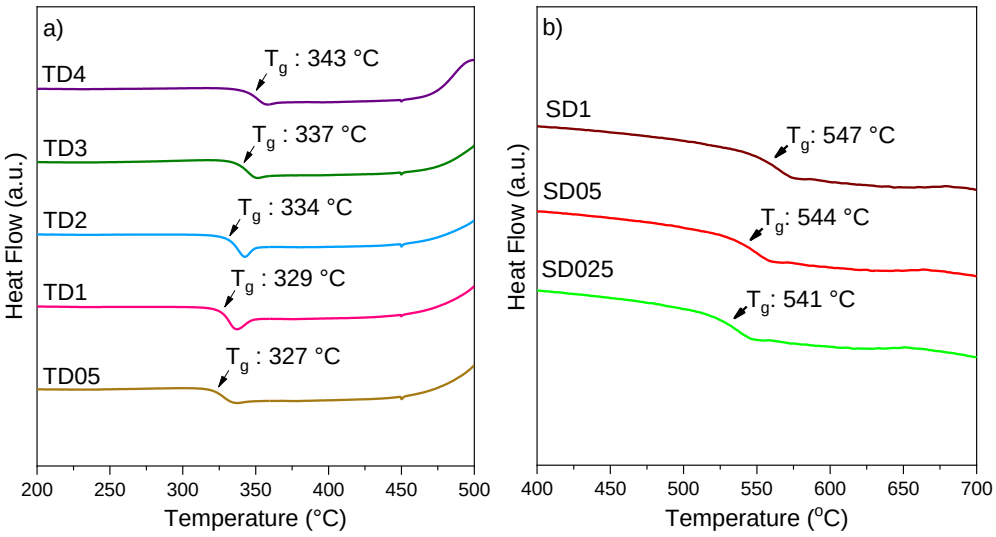


Figure 4.2 DSC results of a) tellurite and b) silicate glasses

The absorption spectrum of tellurite and silicate glasses were measured between 300-1000 nm range and the absorption spectra is given in Figure 4.3. The five absorption peaks of tellurite glasses centered at 452 nm, 474 nm, 757 nm, 806 nm, and 905 nm, which can be seen in Figure 4.3a, are ascribed to the transitions of $^6H_{15/2} \rightarrow {}^4I_{15/2}$, $^6H_{15/2} \rightarrow {}^4F_{9/2}$, $^6H_{15/2} \rightarrow {}^6F_{3/2}$, $^6H_{15/2} \rightarrow {}^6F_{5/2}$ and $^6H_{15/2} \rightarrow {}^6F_{7/2}$ of Dy^{3+}, respectively. [94] The observation of transitions below 410 nm was not possible due to the absorption edge of the tellurite glasses. Additionally, the absorption edge of TD05, TD1, TD2, TD3 and TD4 is located at 420, 424, 429, 433 and 438 nm, respectively. In Figure 4.3b, the absorption spectrum of silicate glasses is presented. The absorption peaks located at 386, 452, 794 and 889 ascribed to the transitions of $^6H_{15/2} \rightarrow {}^4F_{7/2,}$ $^6H_{15/2} \rightarrow {}^4I_{15/2}$, $^6H_{15/2} \rightarrow {}^6F_{5/2}$ and $^6H_{15/2} \rightarrow {}^6F_{7/2}$ respectively. [95] Transitions below 330 nm could not be observed due to the absorption edge of the silicate glasses. Additionally, the absorption edge of SD025, SD05 and SD1 is located at 350, 357 and 362, respectively. No absorption bands were detected in the analyzed region rather than the listed ones in both figures.

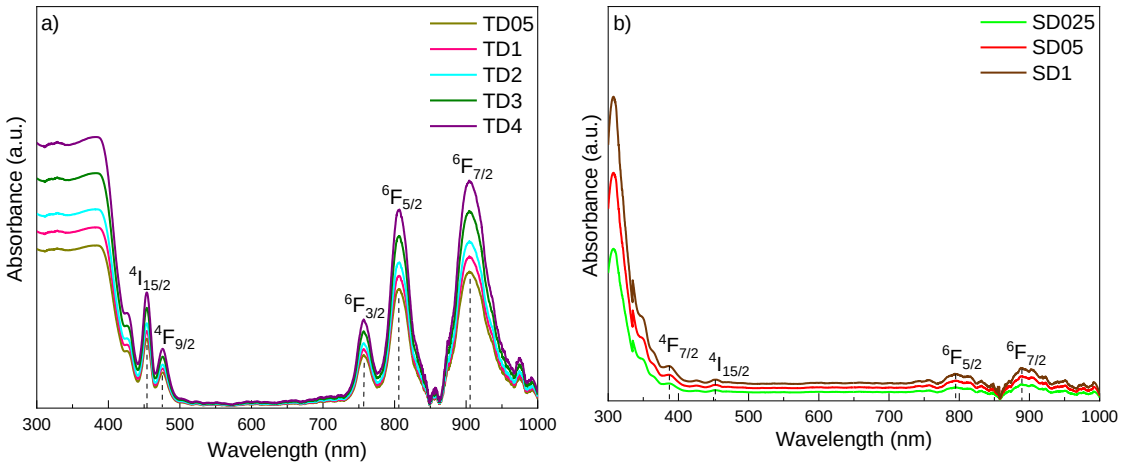


Figure 4.3 Absorption spectra of a) tellurite and b) silicate glasses

Photoluminescence (PL) spectra of rare earth ions exhibit a strong dependence on the excitation wavelength, and in order to determine the most suitable excitation wavelength for the acquisition of white light emission after BCDs coating on the tellurite and silicate glasses, TD3 glass from tellurite and SD05 from silicate system were chosen. PL excitation (PLE) measurements of selected glasses were conducted by monitoring the characteristic yellow emission of Dy^{3+} at 575 nm and the results are given in Figure 4.4. As can be seen from the Figure 4.4a, the PLE spectrum of TD3 glass displays three excitation peaks located at 351 nm, 365 nm, and 388 nm originating from $^6H_{15/2} \rightarrow {}^6P_{7/2}$, $^6H_{15/2} \rightarrow {}^6P_{5/2}$, and $^6H_{15/2} \rightarrow {}^4I_{13/2}$ transitions, respectively. Likewise, the excitation peaks of SD05 glass centered at 324, 349, 363, and 386 nm are ascribed to the $^6H_{15/2} \rightarrow {}^6P_{3/2}$, $^6H_{15/2} \rightarrow {}^6P_{7/2}$, $^6H_{15/2} \rightarrow {}^6P_{5/2}$, and $^6H_{15/2} \rightarrow {}^4F_{7/2}$ transitions, respectively (see Figure 4.4b). [96, 97] According to PLE measurement results, the wavelength of 365 nm was chosen as an excitation wavelength in order to obtain white light emission after BCDs coating.

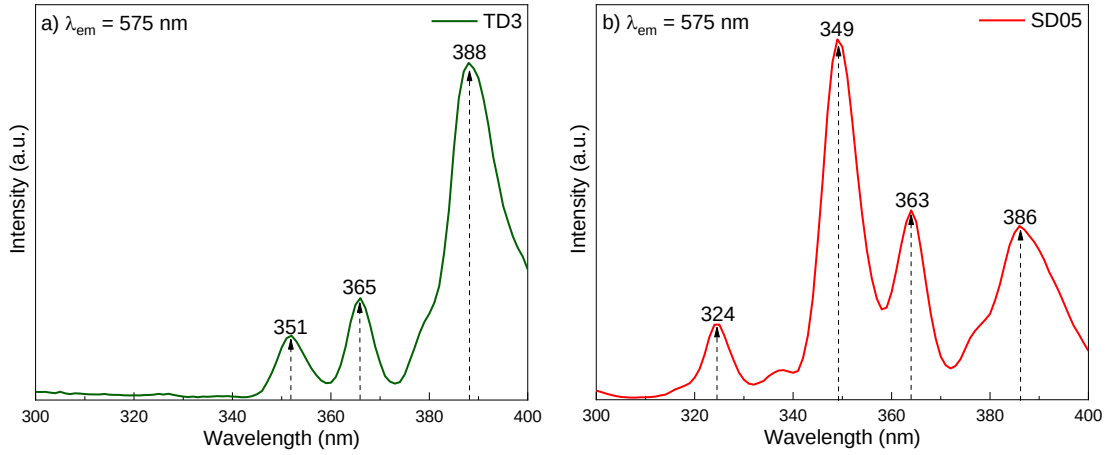


Figure 4.4 PL excitation spectra of a) tellurite and b) silicate glasses

PL emission spectra of Dy^{3+}-doped tellurite and silicate glasses under 365 nm excitation is given in Figure 4.5a and Figure 4.5b, respectively. As can be seen from both spectrums, three emission bands located at 482 nm, 575 nm, and 663 nm corresponding to the $^4F_{9/2} \rightarrow {}^6H_{15/2}$ (blue), $^4F_{9/2} \rightarrow {}^6H_{13/2}$ (yellow) and $^4F_{9/2} \rightarrow {}^6H_{11/2}$ (red) transitions, respectively were detected. The hypersensitive transition of $^4F_{9/2} \rightarrow {}^6H_{13/2}$ which located at 575 nm was more intense than other transitions due to the host-specific dependence of Dy^{3+} ions on the local environment.[98] In Figure 4.5a, the intensity of emission bands was increased with the increasing Dy^{3+} concentration until it reached 3% and for TD4 glass decreased. Also, same behavior occurred for silicate glass system. When Dy^{3+} concentration reached 0.5%, emission intensity of SD1 decreased as represented in Figure 4.5b. However, there was no significant difference in the shape or the peak position of the emission bands for both glass systems. The emission intensity decrement after specific Dy^{3+} ion concentration can be explained with the PL quenching effect due to higher possibility of non-radiative transitions of Dy^{3+} ions in glass matrix which becomes distinguished when the interaction between ions is intensified due to their closer proximity in the glass matrix. Consequently, TD4 and SD1 glasses were eliminated from the coating studies in order to have correct information with regularity for the comparison of glasses.

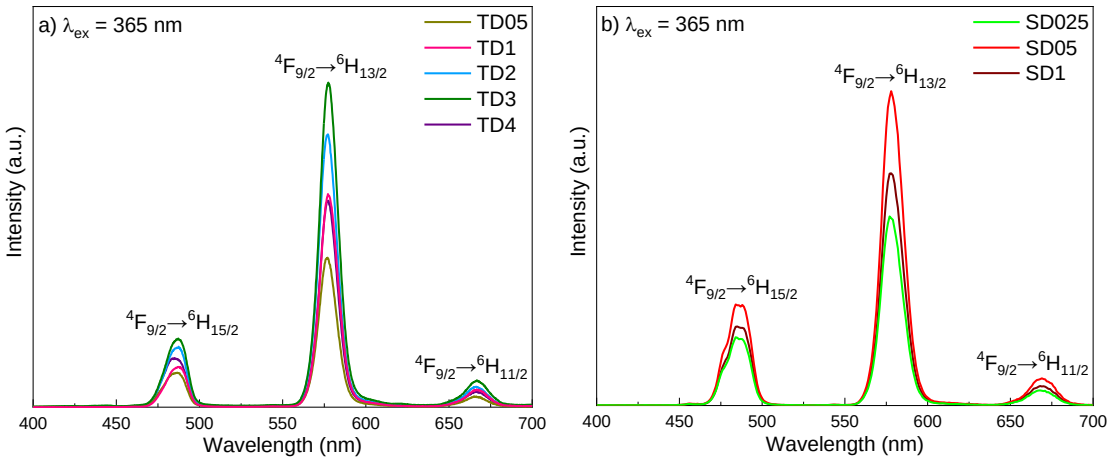


Figure 4.5 PL emission spectra of a) tellurite and b) silicate glasses

The PLQY values of tellurite and silicate glasses calculated from relevant PL emission spectra are listed in Table 4.1. Both tellurite and silicate glasses show increment in their PLQY values with the increasing Dy^{3+} concentration.

Table 4.1 PLQY values of uncoated Dy^{3+}-doped luminescent glasses

Glass System	**Tellurite**					**Silicate**		
Sample	TD05	TD1	TD2	TD3	TD4	SD025	SD05	SD1
PLQY (%)	0.41	1.08	2.24	3.10	4.53	12.65	20.81	24.59

The CIE color chromaticity diagrams of Dy^{3+}-doped tellurite and silicate glasses are given in Figure 4.6a and Figure 4.6b were determined using the obtained data obtained from down-conversion emission spectrums in Figure 4.5. As it can be seen from the CIE diagrams, the coordinates of glasses shifted towards to yellow region with the increasing Dy^{3+} ion concentration.

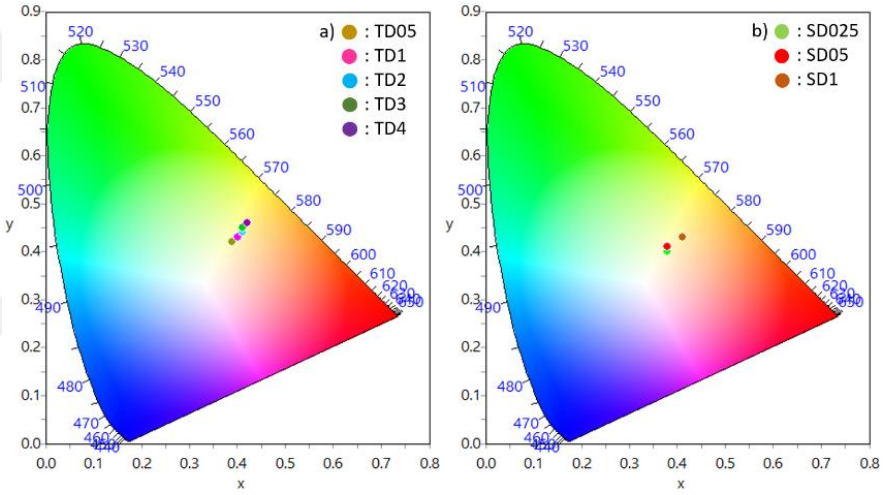


Figure 4.6 CIE color chromaticity coordinates of a) tellurite and b) silicate glasses

Additionally, color coordinates of glasses are listed in Table 4.2 which supports the shift in the coordinates of glasses since x, y values of coordinates increase.

Table 4.2 Color coordinates of tellurite and silicate glasses under 365 nm excitation

Glass System	**Sample**	**Color Coordinates (x, y)**
Tellurite	TD05	0.39, 0.42
	TD1	0.40, 0.43
	TD2	0.41, 0.44
	TD3	0.41, 0.45
	TD4	0.42, 0.46

Table 4.2 Color coordinates of tellurite and silicate glasses under 365 nm excitation (continued…)

Silicate	SD025	0.38, 0.40
	SD05	0.38, 0.41
	SD1	0.41, 0.43

4.1.2 Blue Carbon Dots and BCDs/PVP Solution

The purpose of conducting TGA analysis is to investigate the stability characteristics of BCDs/PVP solution at varying temperatures. The TGA curves of the BCDs/PVP solution represented in Figure 4.7 and it showed a mass loss in two main steps. Within, the temperature range of 25-140 °C, the initial weight loss of the BCDs/PVP solution is observed, primarily attributed to the evaporation of solvents and moisture. The second weight-loss step occurring in the temperature range of 400-500 °C showed that most of the PVP polymer was degraded. Nevertheless, the BCDs/PVP solution showed thermally stable behavior.

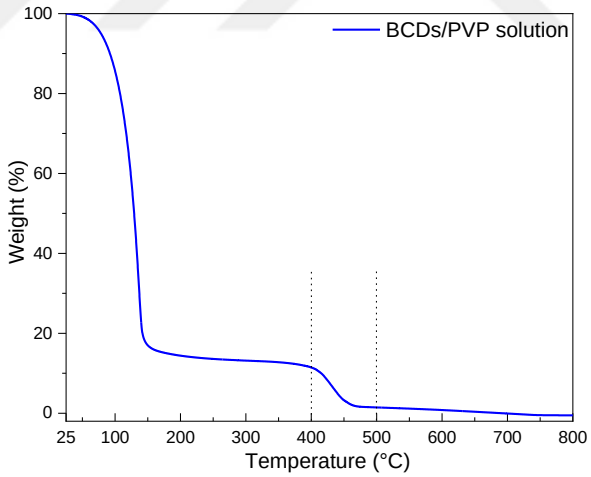


Figure 4.7 TGA curve of BCDs/PVP solution

The optical absorption spectrum of BCDs/PVP solution is given in Figure 4.8. The BCDs/PVP solution was observed to exhibit a very broad absorption band from 325 to 600 nm.

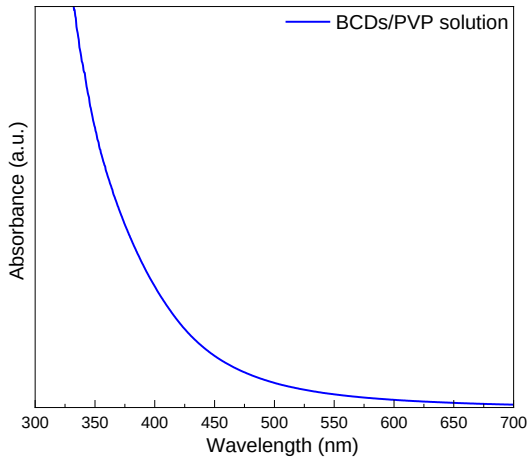
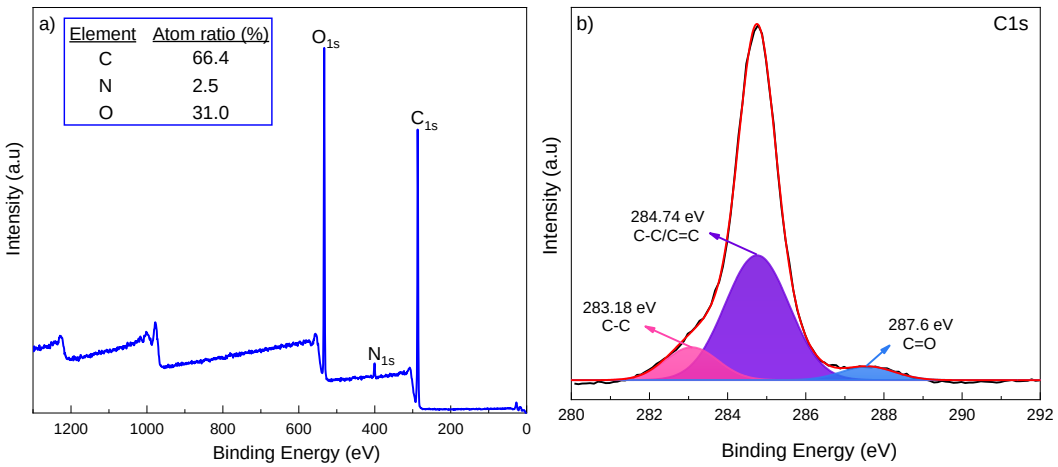


Figure 4.8 The absorption spectrum of BCDs/PVP solution

The XPS analysis is performed to identify elemental compositions and chemical functional groups of BCDs/PVP solution. In Figure 4.9, the binding energies of 287, 401, and 533 eV on the BCDs surface is given in XPS survey spectra which corresponds to C1s, N1s, and O1s, respectively. The elements C (66.4%), O (31.0%), and N (2.5%) that BCDs contains were shown in inset of the Figure 4.9a.[99, 100] The high-resolution XPS spectrum of C1s region showed three peaks 283.18 eV, 284.74 eV, and 287.6 eV, which ascribed to the C-C, C-C/C=C, and C=O groups, respectively, as shown in Figure 4.9b.[100, 101] The high-resolution spectrum of N1s confirmed the presence of pyridinic N (397.4 eV, 398.2 eV, and 398.9 eV) as presented in Figure 4.9c. The high-resolution spectrum of O1s presented in Figure 4.9d confirmed the C=O (529.5 and 530.9 eV), and C-OH/C-O-C (531.6 eV) bonds.[102, 103]



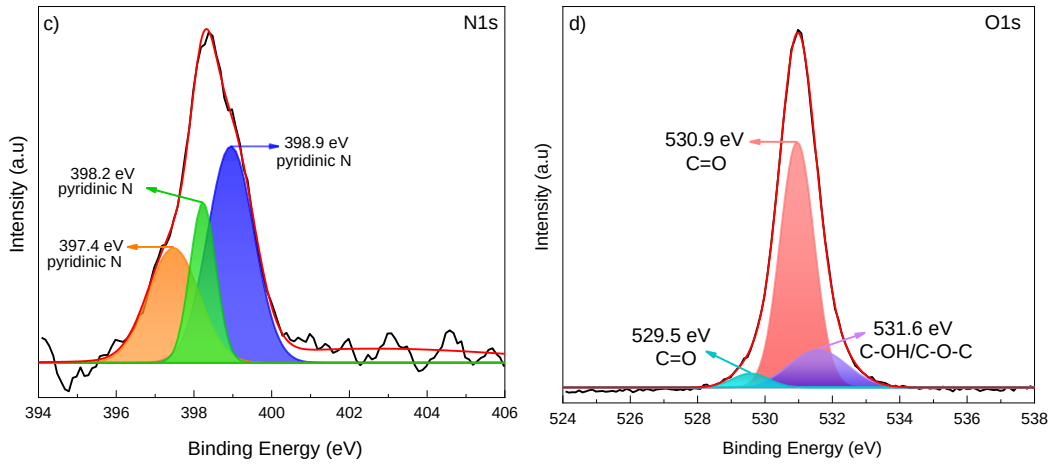


Figure 4.9 a) XPS survey spectrum and high resolution XPS spectra b) C1s, c) N1s, and d) O1s region

The TEM analysis was carried out to characterize the morphology and size of BCDs. The homogeneous distribution of BCDs with good dispersibility can be seen from the general bright-field TEM image in Figure 4.10a. The particle size distribution histogram of BCDs was displayed in Figure 4.10b. As can be seen from this figure, the sizes of BCDs were between 4 nm and 24 nm with an average diameter of 12.49 ± 4.10 nm.

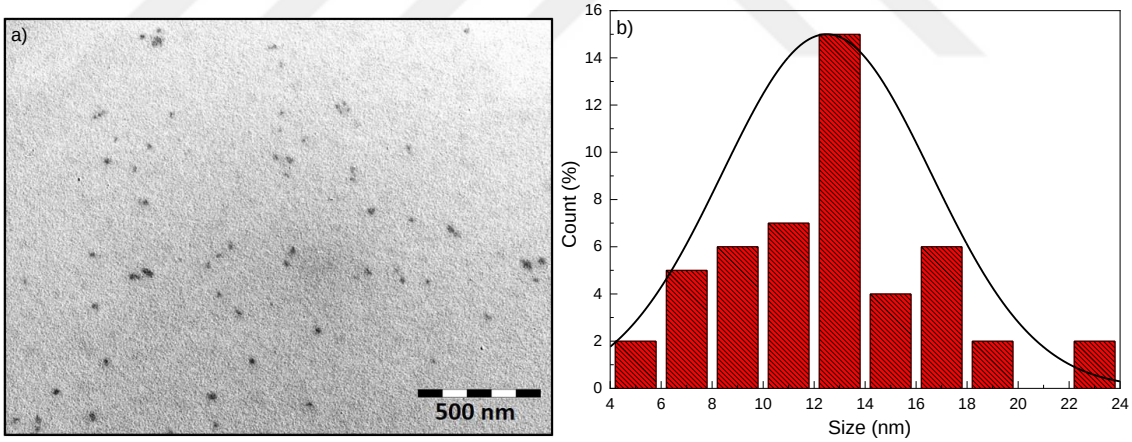


Figure 4.10 a) General bright-field TEM image b) particle size distribution histogram of BCDs

In Figure 4.11, PL excitation (PLE) measurement of the BCDs/PVP solution which is conducted by monitoring the characteristic blue emission at 450 nm. As seen from Figure 4.11, BCDs/PVP solution was suitable for excitation over a wide range in the UV region, including the 365 nm which is a suitable excitation wavelength for Dy^{3+} -doped tellurite and silicate glasses.

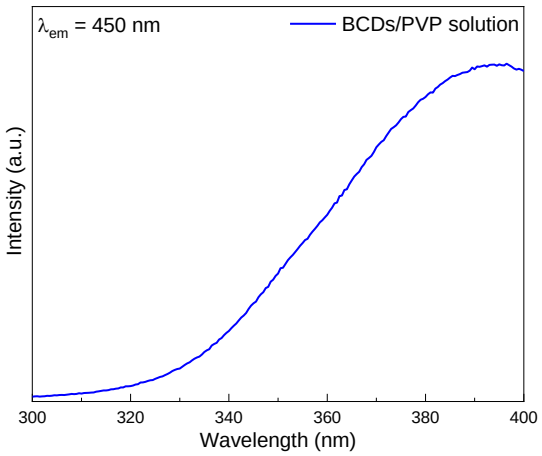


Figure 4.11 PL excitation spectrum of BCDs/PVP solution

PL emission measurement of the BCDs/PVP solution was conducted between the range of 400-750 nm. BCDs/PVP solution demonstrated a broad emission between 400 and 550 nm with an emission peak located at ~450 nm under 365 nm excitation which resulted in intense blue emission as illustrated in Figure 4.12.

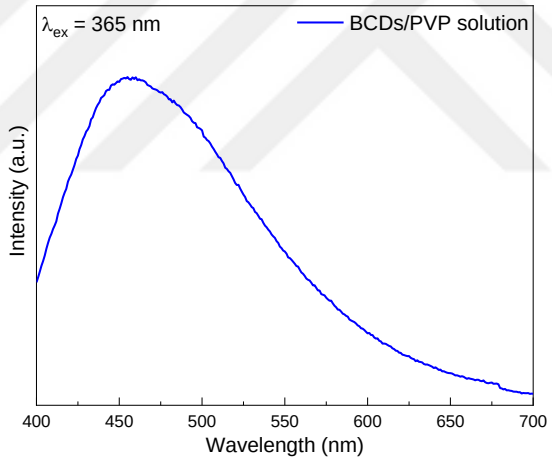


Figure 4.12 PL emission spectrum of BCDs/PVP solution under 365 nm excitation

The PLQY measurement of BCDs/PVP solution under 365 nm excitation is conducted using the obtained data in Figure 4.12 and calculated as 20.83% as illustrated in Figure 4. 13.

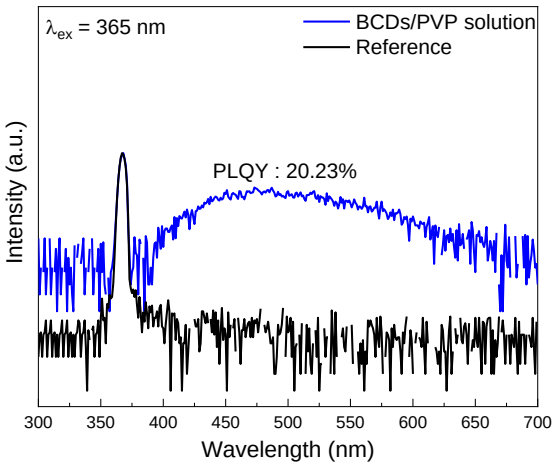


Figure 4. 13 PLQY spectrum of BCDs/PVP solution under 365 nm excitation

The color coordinates of BCDs/PVP solution are given in Figure 4.14 was determined using the obtained data from emission spectrum in Figure 4.12. Color coordinates were calculated as (x = 0.21, y = 0.23).

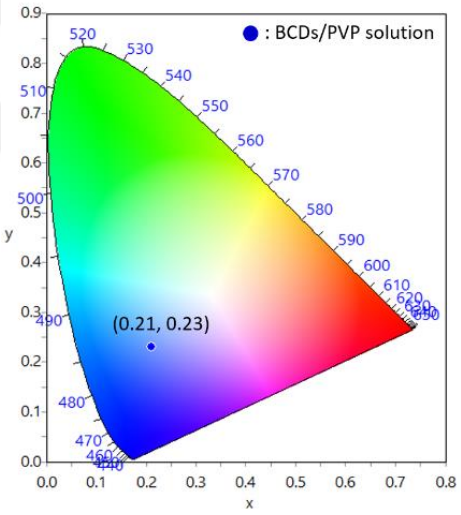


Figure 4.14 CIE color chromaticity diagram of BCDs/PVP solution under 365 nm excitation

Furthermore, the macro image of the BCDs/PVP solution under 365 nm excitation is given in Figure 4.15 which shows the bright blue emission of blue carbon dots.

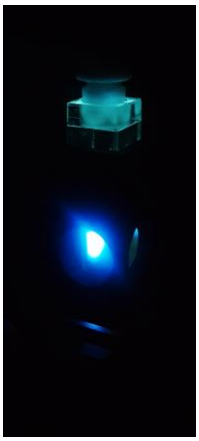
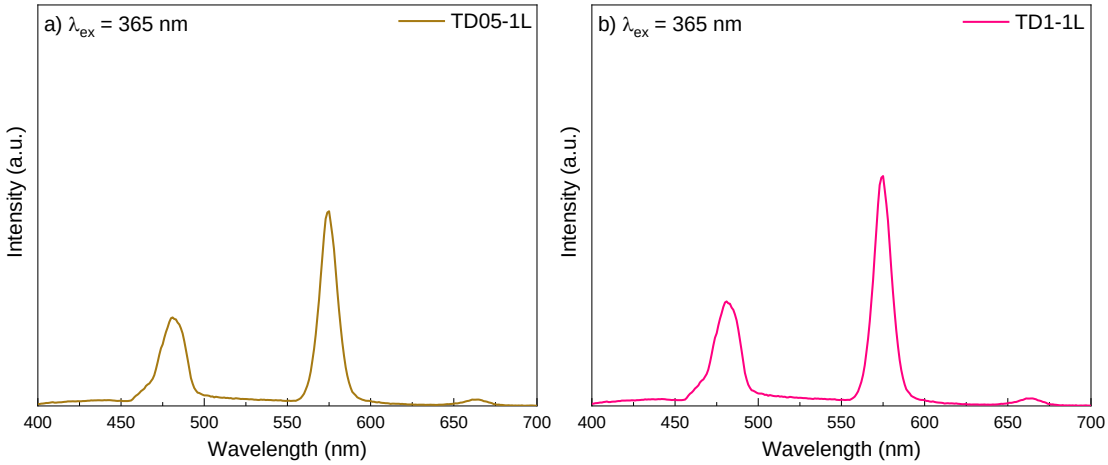


Figure 4.15 The macro image of BCDs/PVP solution under 365 nm excitation

4.1.3 BCDs-coated Luminescent Glasses

4.1.3.1 BCDs-coated Tellurite Glasses

PL emission spectra of one-layer BCDs-coated Dy^{3+}-doped tellurite glasses are given in the Figure 4.16 and the relevant CIE diagrams are illustrated in Figure 4.17 under 365 nm excitation. With a one-layer coating, there was a slight increment in the PL emission of tellurite glasses in the region of 400 – 450 nm, but it is nearly invisible in comparison with the emission intensity of Dy^{3+}-doped tellurite glasses.



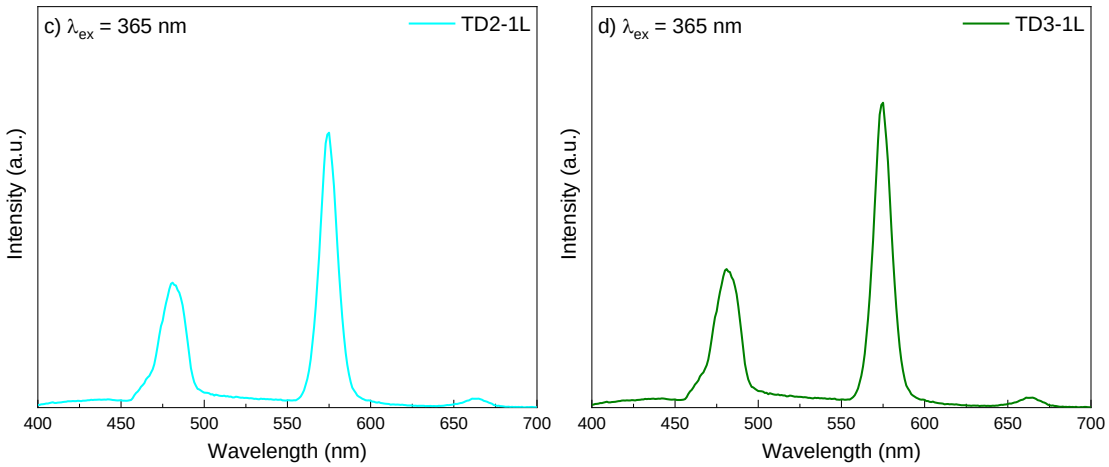
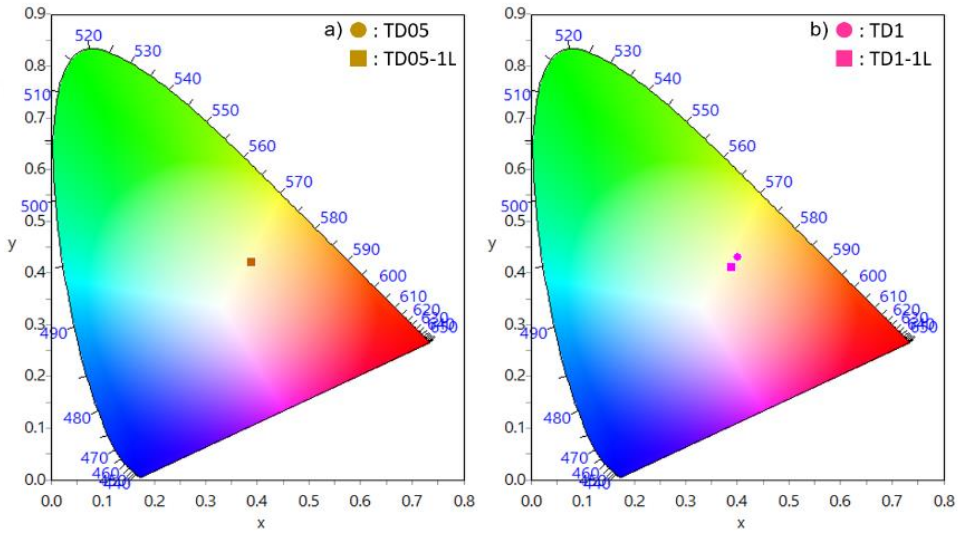


Figure 4.16 PL emission spectra of one-layer BCDs-coated a) TD05-1L b) TD1-L c) TD2-1L d) TD3-1L glasses under 365 nm excitation

Upon one-layer of BCDs-coating, there was no immiscible shift in the CIE coordinates of TD05-1L glass. On the other hand, the rest of the one-layer BCDs-coated tellurite glasses showed a slight shift in their CIE color coordinates as illustrated in Figure 4.17.



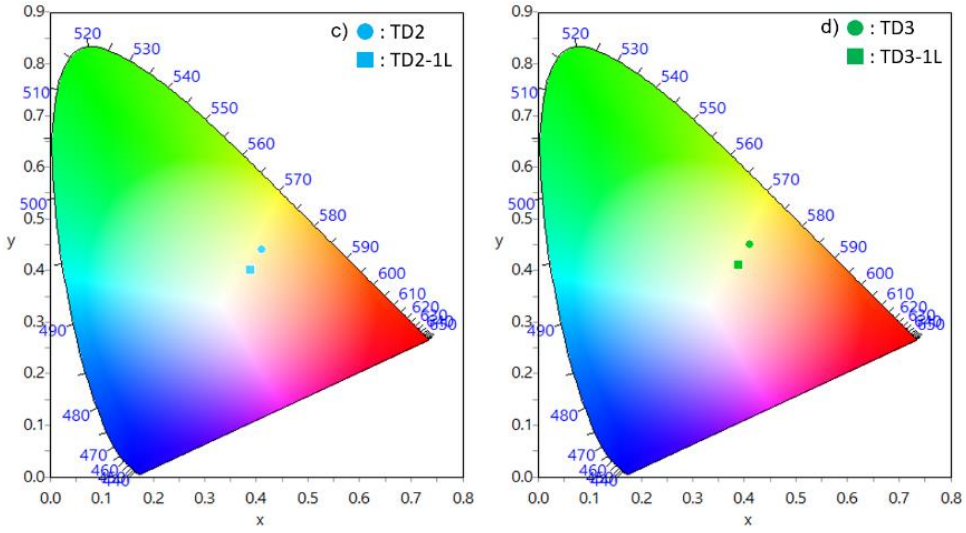


Figure 4.17 CIE diagrams of one-layer BCDs-coated a) TD05-1L b) TD1-1L c) TD2-1L d) TD3-1L glasses under 365 nm excitation

Additionally, relevant color coordinates of glasses are listed in Table 4. 3 as a written proof of CIE diagrams which displayed in Figure 4.17.

Table 4. 3 Color coordinates of one-layer BCDs-coated tellurite glasses

Sample	Color Coordinates (x, y)
TD05-1L	0.39, 0.42
TD1-1L	0.39, 0.41
TD2-1L	0.39, 0.40
TD3-1L	0.39, 0.41

PL emission spectra of two-layers BCDs-coated Dy^{3+}-doped tellurite glasses are given in the Figure 4.17 and the relevant CIE diagrams in Figure 4.18 under 365 nm excitation. With two-layers coating there was a visible increment of the PL emission of tellurite glasses in the region of 400 – 450 nm.

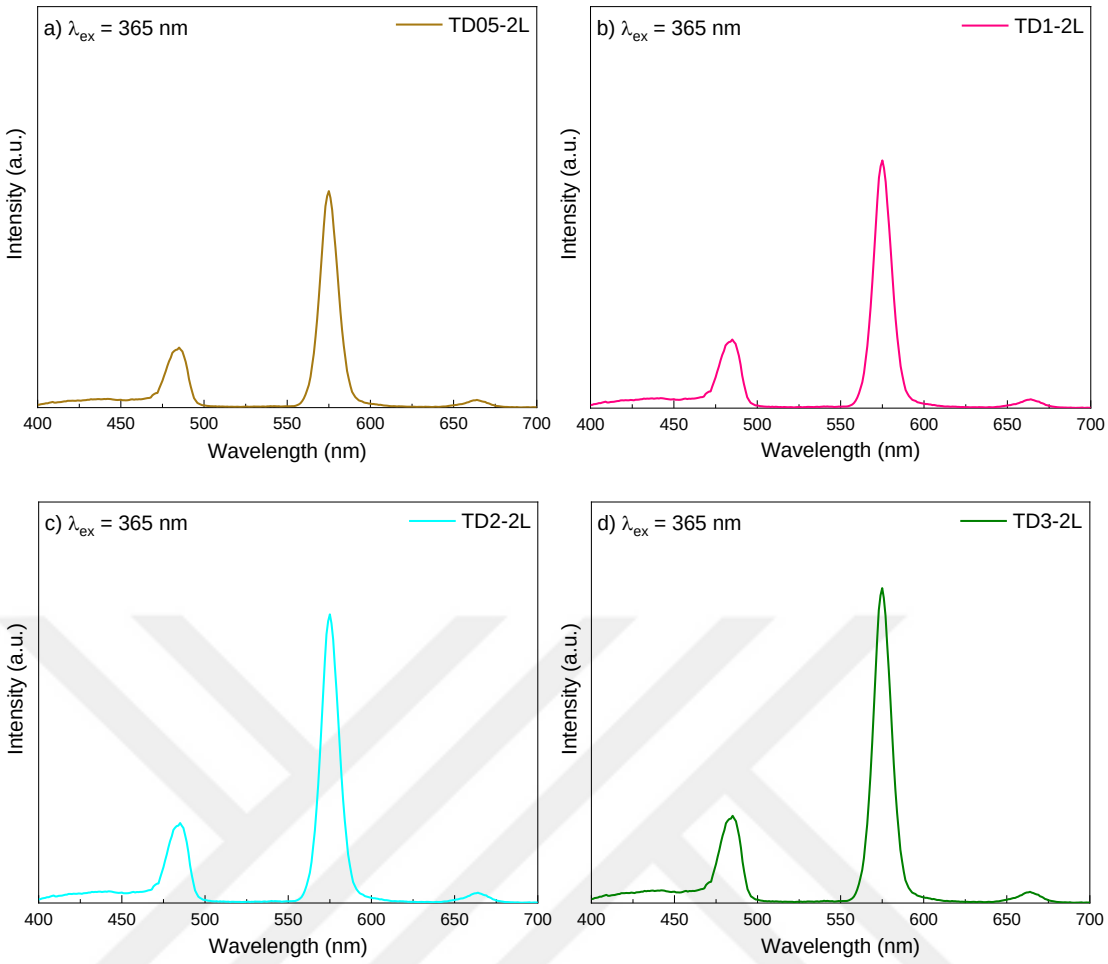
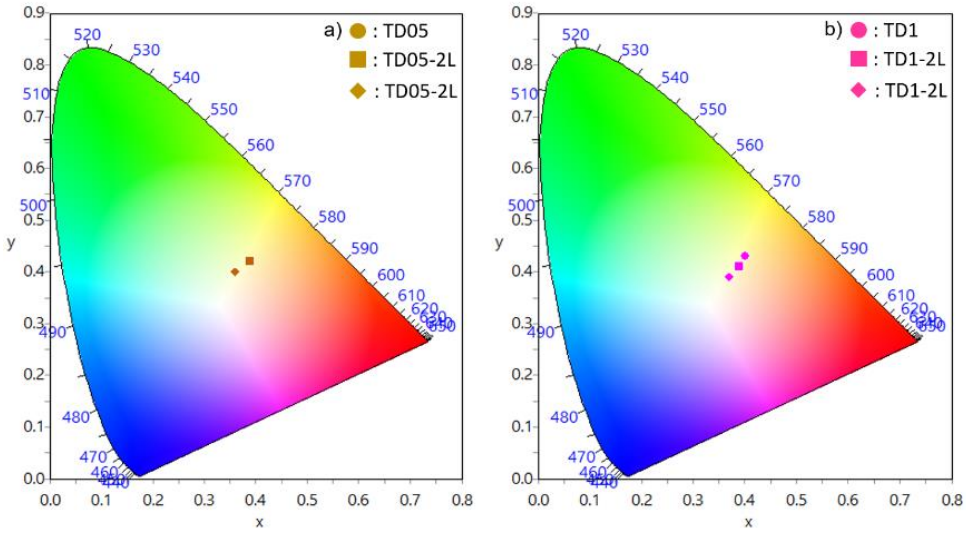


Figure 4.18 PL emission spectra of two-layers BCDs-coated a) TD05-2L b) TD1-2L c) TD2-2L d) TD3-2L glasses under 365 nm excitation

Upon two-layers of BCDs-coating, all glasses showed a visible shift in their CIE color coordinates as illustrated in Figure 4.19.



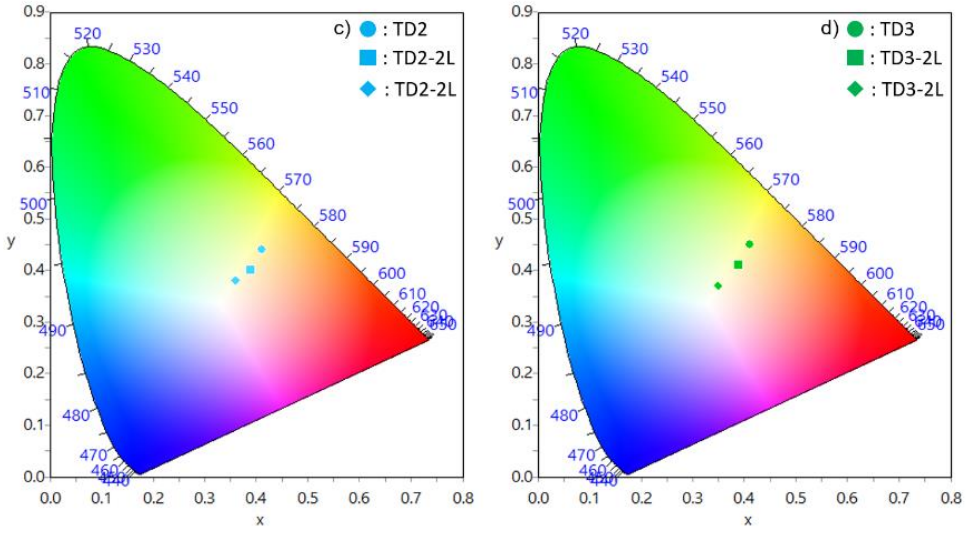


Figure 4.19 CIE diagrams of two-layers BCDs-coated a) TD05-2L b) TD1-2L c) TD2-2L d) TD3-2L glasses under 365 nm excitation

Additionally, relevant color coordinates of glasses are listed in Table 4. 4 as a written proof of CIE diagrams which displayed in Figure 4.19.

Table 4. 4 Color coordinates of two-layers BCDs-coated tellurite glasses

Sample	Color Coordinates (x, y)
TD05-2L	0.36, 0.40
TD1-2L	0.37, 0.39
TD2-2L	0.36, 0.38
TD3-2L	0.35, 0.37

PL emission spectra of three-layers BCDs-coated Dy^{3+}-doped tellurite glasses are given in the Figure 4.20 and the relevant CIE diagrams in Figure 4.21 under 365 nm excitation. With three-layers coating, there was a significantly higher increment in the PL emission of tellurite glasses in the region of 400 – 450 nm than with two-layers of BCDs-coated glasses.

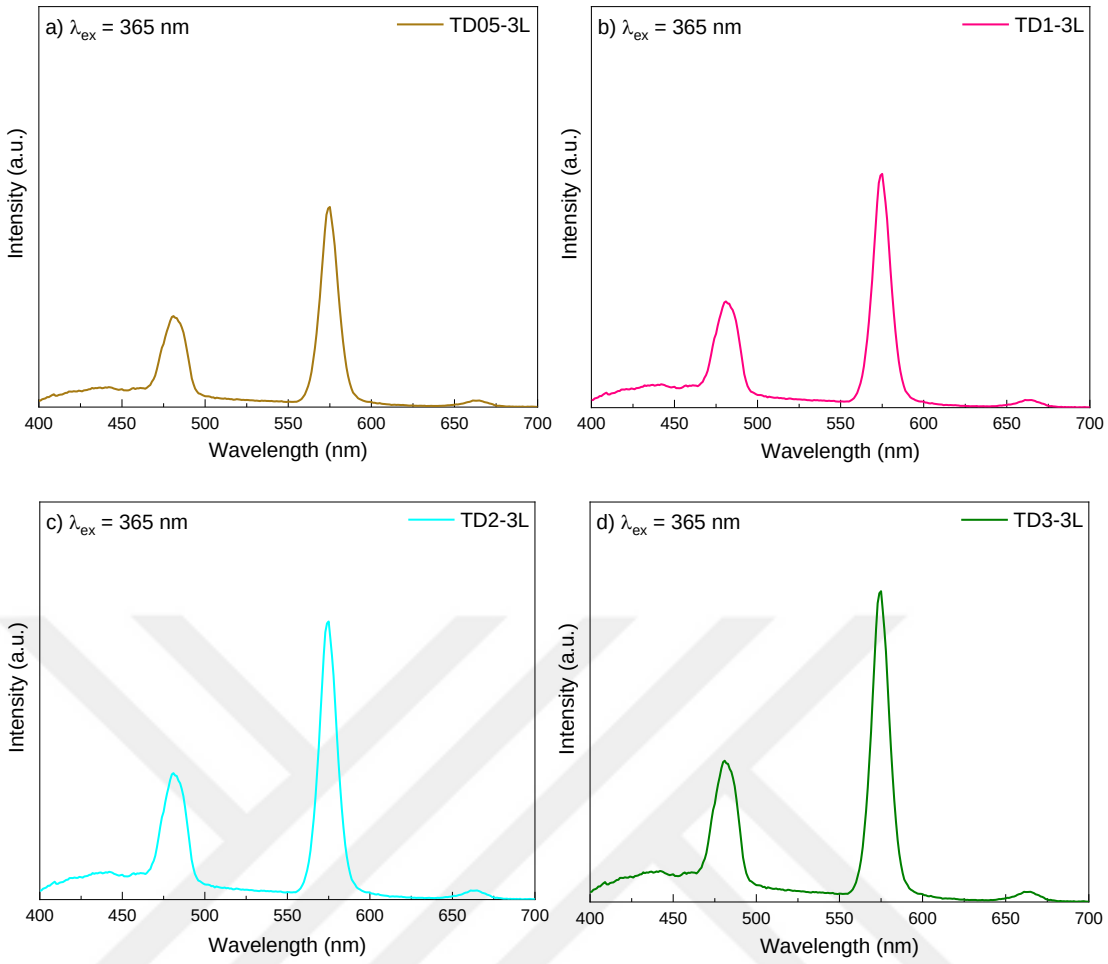
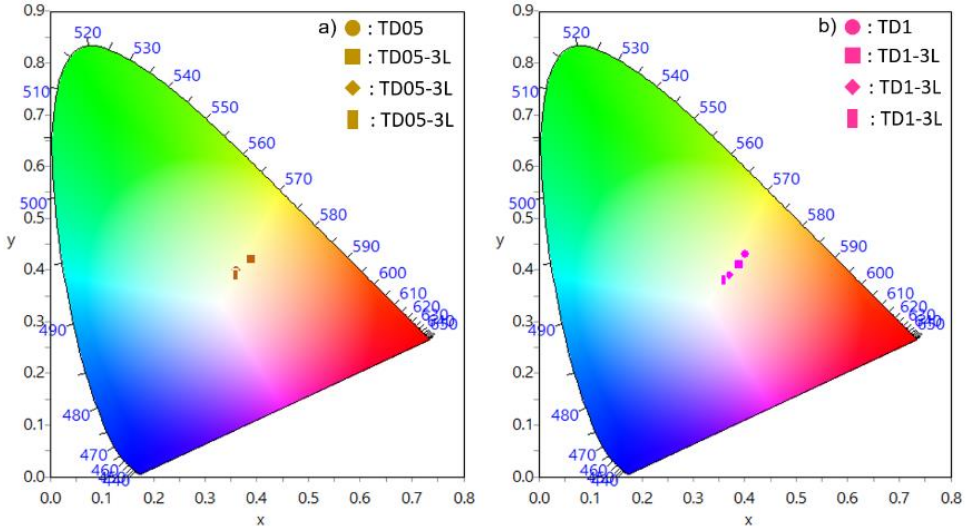


Figure 4.20 PL emission spectra of three-layers BCDs-coated a) TD05-3L b) TD1-3L c) TD2-3L d) TD3-3L glasses under 365 nm excitation

Upon three-layers of BCDs-coating, all glasses showed a greater shift from yellow region to white region in the CIE color coordinates than with two-layers of BCDs-coating as illustrated in Figure 4.21.



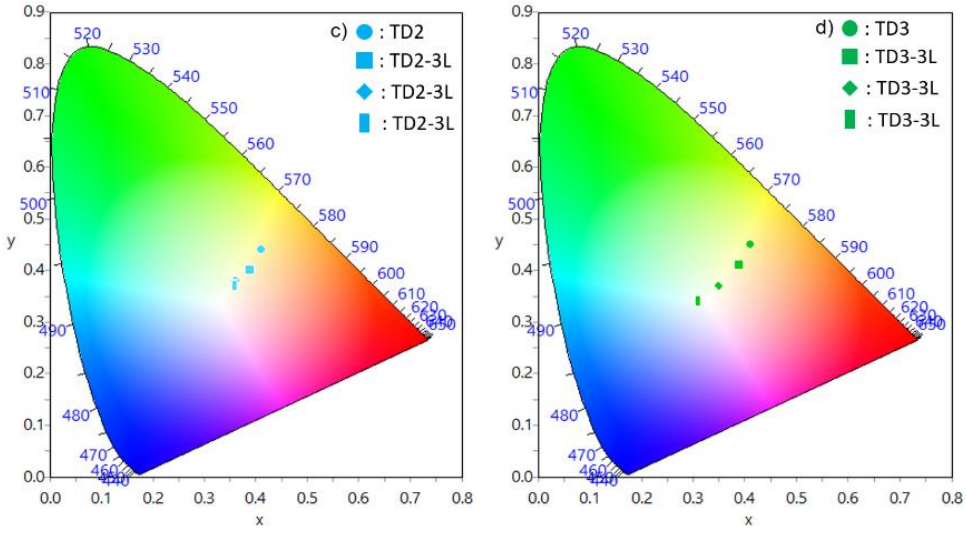


Figure 4.21 CIE diagrams of three-layers BCDs-coated a) TD05-3L b) TD1-3L c) TD2-3L d) TD3-3L glasses under 365 nm excitation

Additionally, relevant color coordinates of glasses are listed in Table 4. 5 as a written proof of CIE diagrams which displayed in Figure 4.21.

Table 4. 5 Color coordinates of three-layers BCDs-coated tellurite glasses

Sample	Color Coordinates (x, y)
TD05-3L	0.36, 0.39
TD1-3L	0.37, 0.38
TD2-3L	0.36, 0.37
TD3-3L	0.31, 0.33

4.1.3.2 BCDs-coated Silicate Glasses

PL emission spectra of one-layer BCDs-coated Dy^{3+}-doped silicate glasses are given in the Figure 4.24 and the relevant CIE diagrams are illustrated in Figure 4.25 under 365 nm excitation. With a one-layer coating, there was a slight increment in the PL emission of tellurite glasses in the region of 400 – 450 nm, but it is nearly invisible in comparison with the emission intensity of Dy^{3+}-doped silicate glasses.

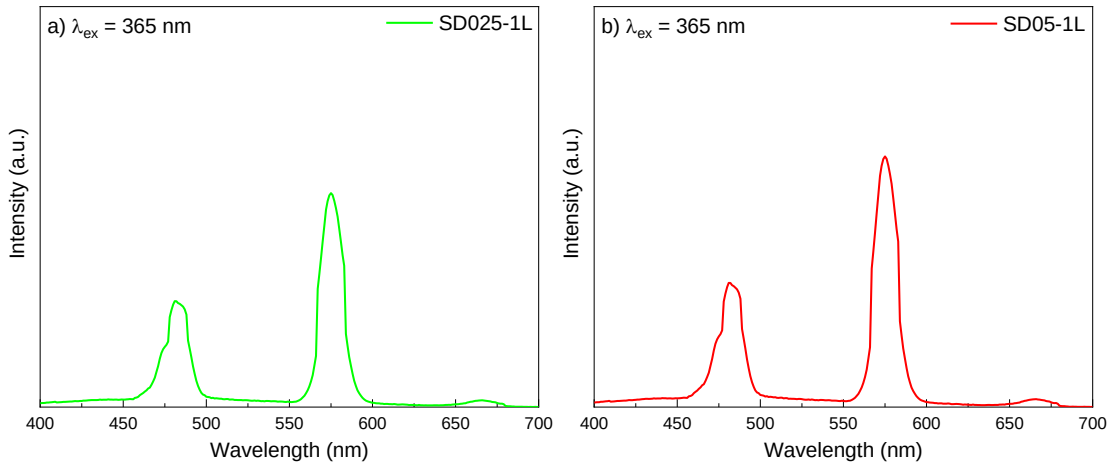


Figure 4.22 PL emission spectra of one-layer BCDs-coated a) SD025-1L b) SD05-1L glasses under 365 nm excitation

Upon one-layer of BCDs-coating, there was no immiscible shift in the CIE coordinates of SD025-1L glass. On the other hand, SD05-1L glass showed a slight shift in its CIE color coordinates as illustrated in Figure 4.25.

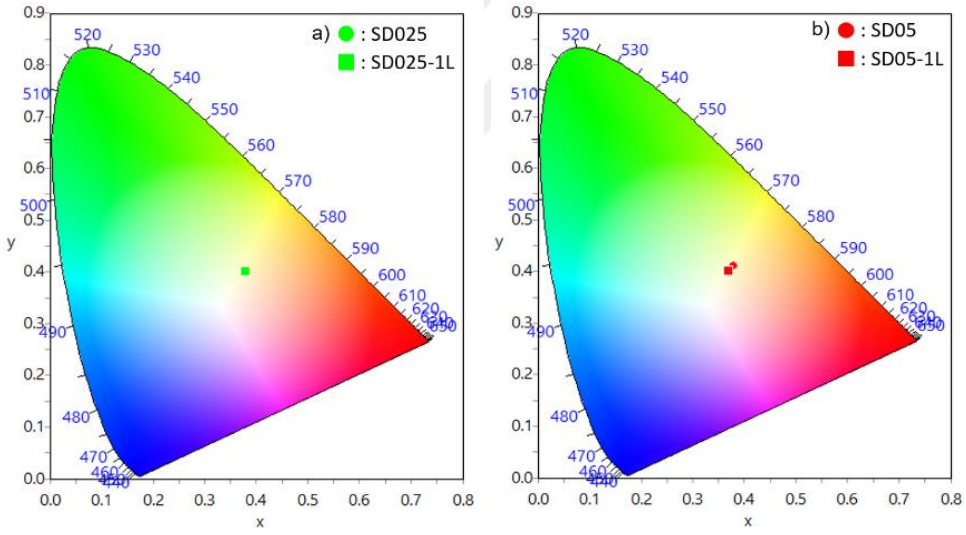


Figure 4.23 CIE diagrams of one-layer BCDs-coated a) SD025-1L and b) SD05-1L glasses under 365 nm excitation

Additionally, relevant color coordinates of glasses are listed in Table 4. 6 as a written proof of CIE diagrams which displayed in Figure 4.25.

Table 4. 6 Color coordinates of one-layer BCDs-coated silicate glasses

Sample	Color Coordinates (x, y)
SD025-1L	0.38, 0.40
SD05-1L	0.37, 0.40

PL emission spectra of two-layers BCDs-coated Dy^{3+}-doped silicate glasses are given in the Figure 4.26 and the relevant CIE diagrams in Figure 4.27 under 365 nm excitation. With two-layers coating there was a visible increment of the PL emission of silicate glasses in the region of 400 – 450 nm.

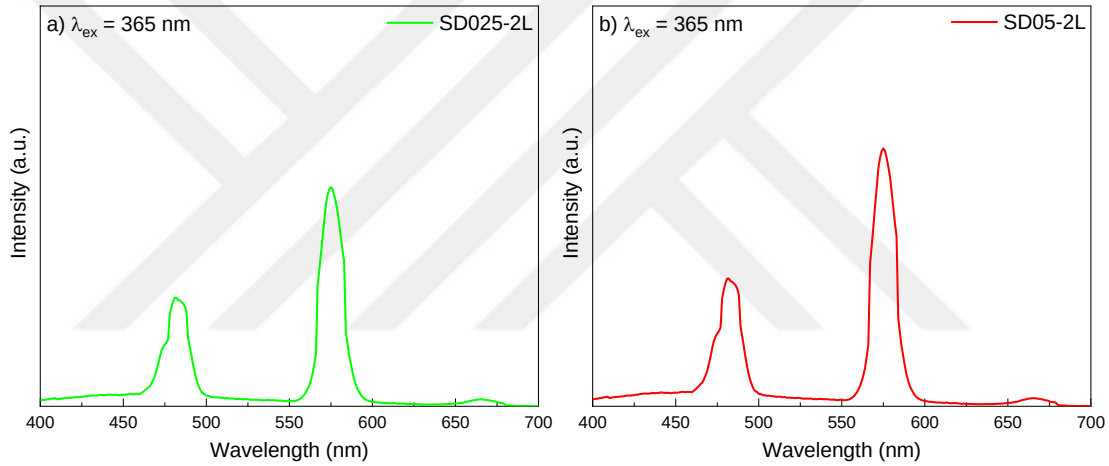


Figure 4.24 PL emission spectra of two-layers BCDs-coated a) SD025-2L b) SD05-2L glasses under 365 nm excitation

Upon two-layers of BCDs-coating, all glasses showed a visible shift in their CIE color coordinates as illustrated in Figure 4.27.

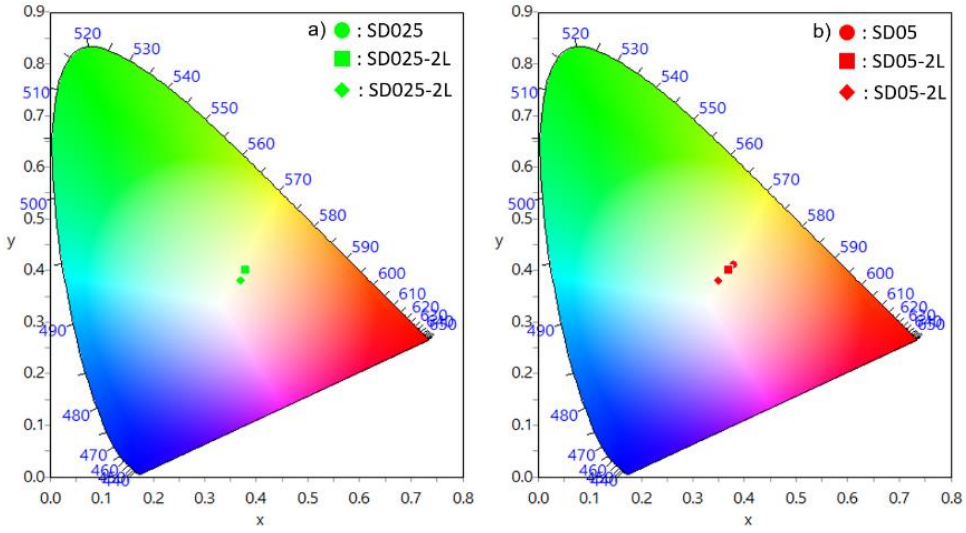


Figure 4.25 CIE diagrams of two-layers BCDs-coated a) SD025-2L and b) SD05-2L glasses under 365 nm excitation

Additionally, relevant color coordinates of glasses are listed in Table 4. 7 as a written proof of CIE diagrams which displayed in Figure 4.27.

Table 4. 7 Color coordinates of two-layers BCDs-coated silicate glasses

Sample	Color Coordinates (x, y)
SD025-2L	0.37, 0.38
SD05-2L	0.35, 0.38

PL emission spectra of three-layers BCDs-coated Dy^{3+}-doped silicate glasses are given in the Figure 4.28 and the relevant CIE diagrams in Figure 4.29 under 365 nm excitation. With three-layers coating, there was a significantly higher increment in the PL emission of silicate glasses in the region of 400 – 450 nm than with two-layers of BCDs-coated glasses.

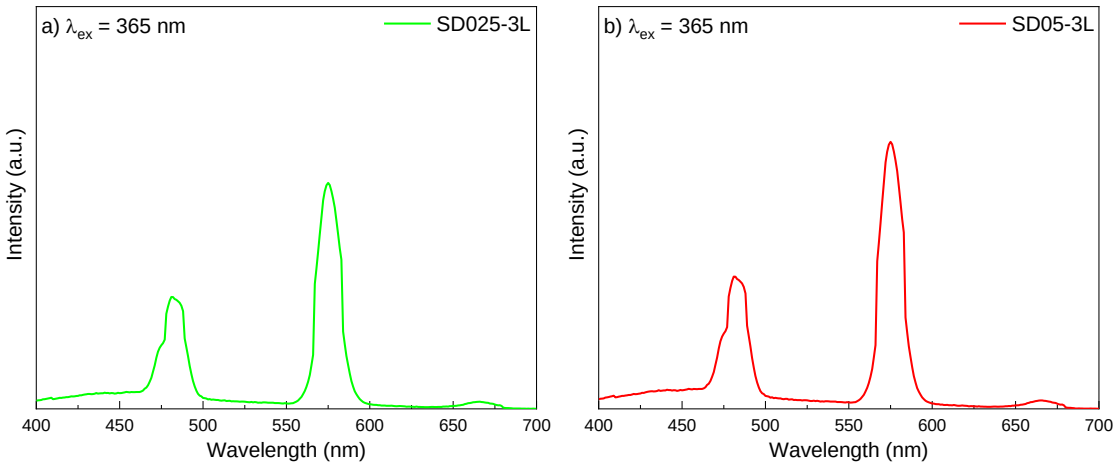


Figure 4.26 PL emission spectra of three-layers BCDs-coated a) SD025-1L b) SD05-1L glasses under 365 nm excitation

Upon three-layers of BCDs-coating, all glasses showed a greater shift from yellow region to white region in the CIE color coordinates than with two-layers of BCDs-coating as illustrated in Figure 4.29.

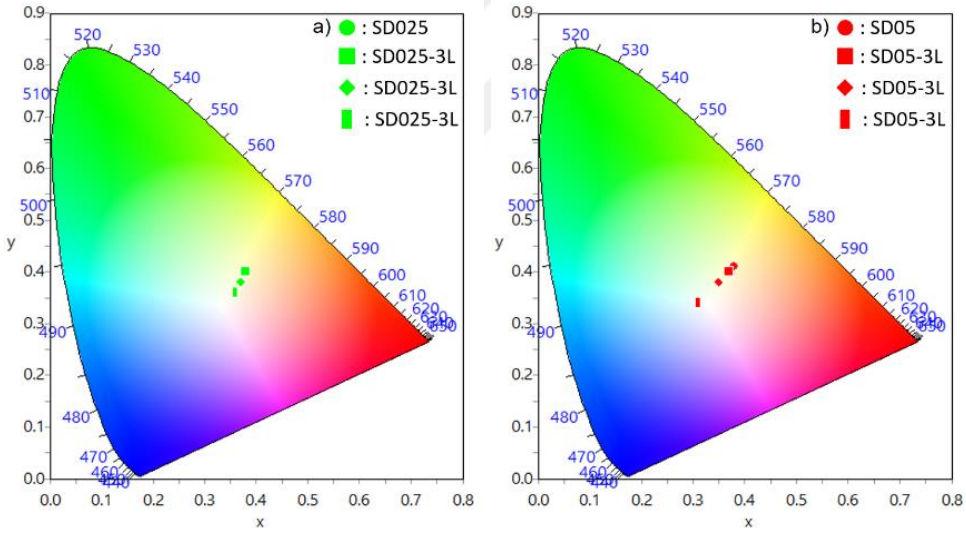


Figure 4.27 CIE diagrams of three-layers BCDs-coated a) SD025-3L and b) SD05-3L glasses under 365 nm excitation

Additionally, relevant color coordinates of glasses are listed in Table 4. 8 as a written proof of CIE diagrams which displayed in Figure 4.29.

Table 4. 8 Color coordinates of three-layers BCDs-coated silicate glasses

Sample	Color Coordinates (x, y)
SD025-3L	0.36, 0.36
SD05-3L	0.31, 0.34

4.1.4 White Light Emission – The Comparison of TD3-3L and SD05-3L Glasses

In order to discuss the obtained experimental results, the samples with the white light emission by means of Dy^{3+}-doped TD3-3L and SD05-3L were compared with the uncoated glasses, together. Additionally, the coating thickness, surface morphology and temperature-dependent PL emission behavior of selected samples were investigated separately.

PL emission spectra of BCDs-coated TD3-3L and SD05-3L glasses are depicted along with their uncoated versions together for better comparison of the emission intensities in Figure 4.28a and Figure 4.28b, respectively. As a result of excitation three characteristic emission bands of Dy^{3+} is located at 482 nm, 575 nm, and 663 nm corresponding to the $^4F_{9/2} \rightarrow {}^6H_{15/2}$ (blue), $^4F_{9/2} \rightarrow {}^6H_{13/2}$ (yellow) and $^4F_{9/2} \rightarrow {}^6H_{11/2}$ (red) transitions, respectively for all of the glasses as it can be seen from Figure 4.28a and Figure 4.28b. Moreover, there is no significant difference in the shape or position of the emission bands for both glass systems. Only, the transition of $^4F_{9/2} \rightarrow {}^6H_{13/2}$ is relatively more intense than other transitions since it is hypersensitive which is due to the strong dependence of the Dy^{3+} ion on the local environment. After BCDs coating was applied to glass surfaces and the PL spectra of uncoated and BCDs-coated glasses were compared, a significant enhancement of the PL emission intensity between 400 and 550 nm was observed on the glass surfaces of TD3-3L and SD05-3L, which can be seen from Figure 4.28a and Figure 4.28b, respectively. The increment in the emission intensity of the blue region also confirms the presence of the BCDs-coating on the glass surfaces since Dy^{3+} ion does not have any other emission in the blue region. Additionally, after BCDs-coating no shift occurred in the wavelengths of emission peaks for both glass systems.

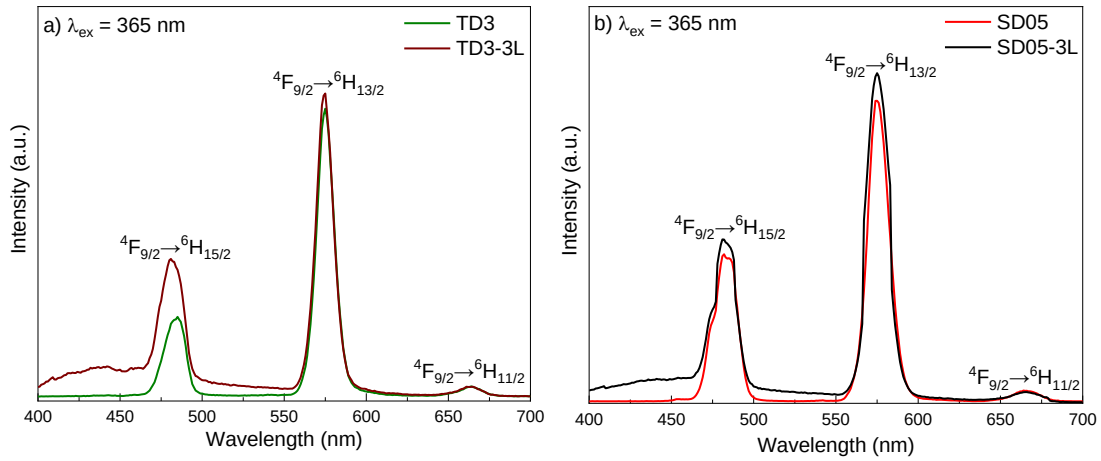


Figure 4.28 PL emission spectra of a) TD3 & TD3-3L b) SD05 & SD05-3L glasses

For better comparison of how white light is achieved after several layers, PL emission intensities of tellurite and silicate glasses with the increasing layers of BCDs-coating are given in Figure 4.29a and Figure 4.29b, respectively. PL emission results of BCDs-coated tellurite and silicate glasses show a systematical enhancement in intensity by increasing the number of coating layers in both glasses. Additionally, it is obvious that BCDs aggregation, which is a typical behavior of aggregated fluorescent carbon dots due to AIQ as stated before, does not occur as there is no indication of quenching.

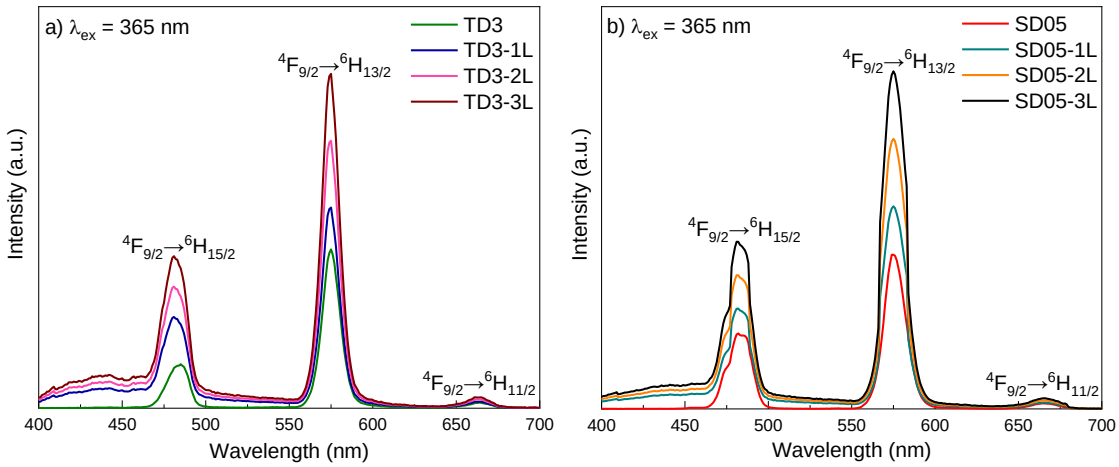


Figure 4.29 PL emission spectra of BCDs-coated a) TD3 and b) SD05 glasses

The PLQY measurements of three-layers BCDs-coated TD3-3L and SD05-3L glasses under 365 nm excitation are conducted using the obtained data in Figure 4.20 and Figure 4.26, and illustrated in Figure 4. 30. Before BCDs-coating PLQY values of TD3 and SD glasses were 3.10% and 20.81%, respectively. After three-layers of BCDs-coating, PLQY

values are calculated as 5.62 % and 31.49 %, respectively. Since PLQY is calculated as overall amount of emissions obtained from coated glasses, the enhancement in PLQY values can be explained by the boosted emission of Dy^{3+} ions by BCDs coating in addition to the emissions originating from both Dy^{3+}-doped glasses and BCDs coating. As a result, both glasses showed nearly 50% increment in their PLQY values.

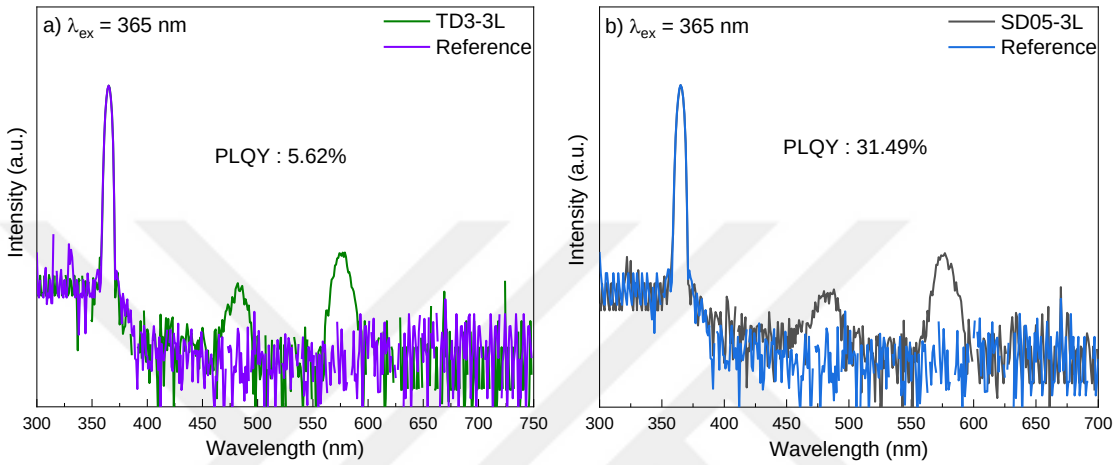


Figure 4. 30 PLQY spectra of a) TD3-3L and b) SD05-3L glasses under 365 nm excitation

For additional information, the increment in PLQY values can be explained with also the radiative energy transfer mechanism which occurs when emission and absorption spectra overlaps. The BCDs/PVP solution exhibits a wide photoluminescence (PL) spectrum, with a prominent emission peak centered around ~450 nm. Furthermore, absorption band of Dy^{3+}-doped tellurite and silicate glasses is located at 452 nm and ascribed to $^6H_{15/2} \rightarrow {}^4I_{15/2}$ transition of Dy^{3+}. The emission peak of BCDs/PVP and absorption peak of Dy^{3+} ion coincide nearly at the same wavelength as illustrated in Figure 4. 31a and Figure 4. 31b. Consequently, the emission from BCDs coating can be absorbed and re-emitted by Dy^{3+} ions and as a result, BCDs coated glasses exhibit enhanced PL emissions ultimately causing an increase in the PLQY values.

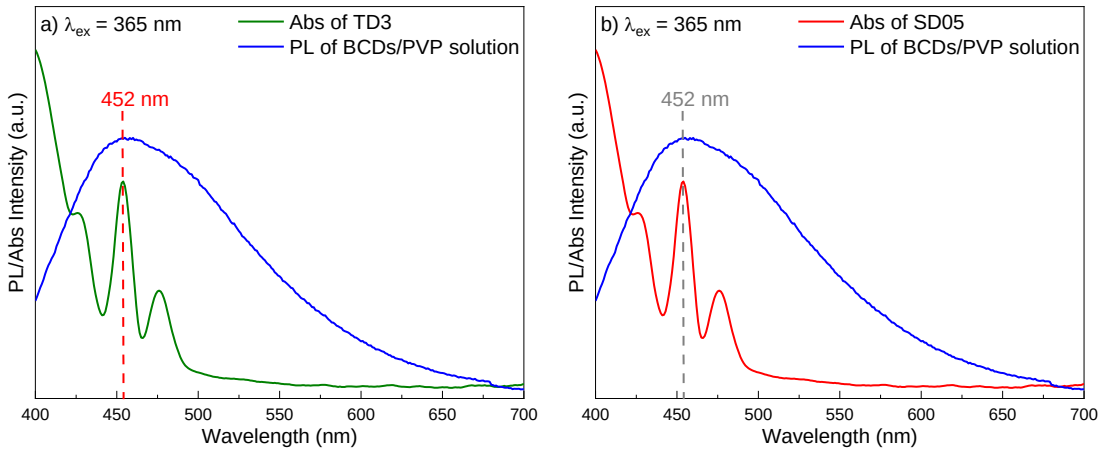


Figure 4. 31 PL and absorbance spectra of a) TD3 and b) SD05 glasses under 365 nm excitation

The CIE color coordinates (x,y) are derived from the intensities of emission specral profiles displayed in Figure 4.32a and Figure 4.32b. The corresponding CIE chromaticity diagrams of uncoated and BCDs-coated tellurite and silicate glasses are given in Figure 4.32a and Figure 4.32b. The CIE color coordinates of TD3 glass is located at (x = 0.41, y = 0.45) and after BCDs-coating TD3-3L glass shifted to the (x = 0.31, y = 0.33) as seen from the Figure 4.32a. The CIE color coordinates of SD05 glass is located at (x = 0.38, y = 0.41) and after BCDs-coating SD05-3L glass shifted to the (x = 0.31, y = 0.34) as seen from the Figure 4.32b. The uncoated glasses were in the yellow region of the CIE chromaticity diagram and upon the application of BCDs-coating, BCDs-coated tellurite and silicate glasses shifted to the white region of the diagram. However, a further movement observed in tellurite glass from the original coordinates to the white region than silicate glass. As a result, the same layer of BCDs-coating can result in different PL emission intensities for tellurite and silicate glass systems.

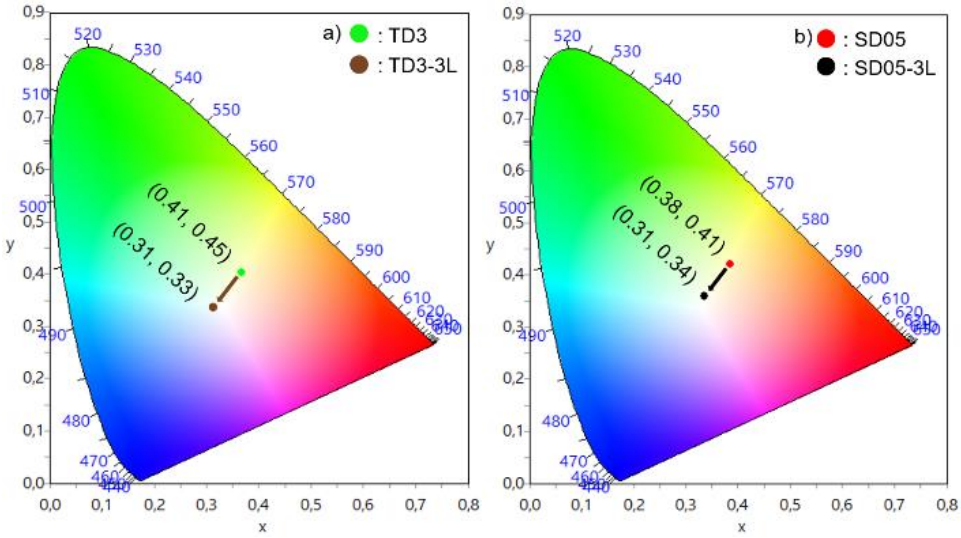


Figure 4.32 CIE chromaticity diagrams of a) TD3 & TD3-3L and b) SD05 & SD05-3L glasses under 365 nm excitation

The white light emission obtained from TD3-3L and SD05-3L glasses can be seen from the macro images in Figure 4.33. The macro images demonstrated that under 365 nm excitation, uncoated glasses emit yellow color and BCDs-coated glasses emit white light.

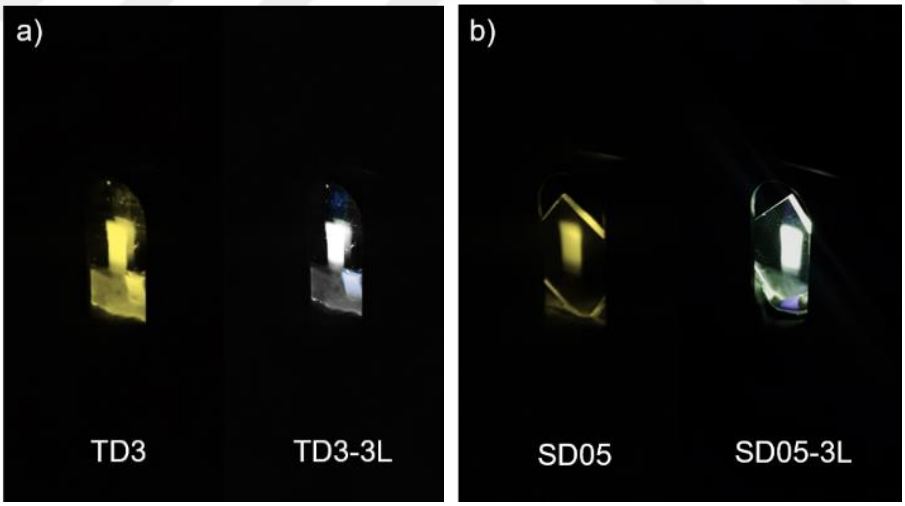


Figure 4.33 The macro images of a) TD3 & TD3-3L and b) SD05 & SD05-3L glasses under 365 nm excitation

In addition to the CIE color coordinates, to better understand the colorimetric properties of uncoated and BCDs-coated tellurite and silicate glasses, the quality of white light is also evaluated in terms of colorimetric parameters such as CCT, CRI, and color purity which are given in Table 4.9. The CCT values of TD3 and SD05 glasses are calculated

as 3657 and 4044 K, respectively. On the other hand, BCDs-coated TD3-3L and SD05-3L glasses are calculated as 5518 and 5136 K, respectively, which are comparable to the CCT values of commercial white LEDs (> 4000 K). [104, 105] The CRI values of uncoated tellurite and silicate glasses were 8 and 6, respectively, which nearly doubled to 17 and 19, respectively, when BCDs-coating was applied. The lower CRI values of uncoated glasses can be explained with the insufficient blue emission of Dy^{3+}-doped glasses. Furthermore, the color purity of uncoated TD3 and SD05 glasses is measured as 64.8 % and 49.2 %, respectively. A dramatic decrease was observed in the color purity values of TD3-3L (7.7 %) and SD05-3L (10.2 %) glasses, which confirms that the glasses displayed white light since pure white light has a color purity of 0%.

Table 4.9 Colorimetric properties of selected glasses before & after BCDs-coating

Glass System	Sample	CCT (K)	CRI	Color Purity (%)
Tellurite	TD3	3657	8	64.8
	TD3-3L	5518	17	7.7
Silicate	SD05	4044	6	49.2
	SD05-3L	5316	19	10.2

The surface morphology TD3-3L and SD05-3L glasses were analyzed by SEM and results show glasses have mostly uniformly distributed surface after BCDs-coating as presented in Figure 4.34a and Figure 4.34b, respectively. Additionally, the cross-sectional SEM images displays the coating thickness of TD3-3L and SD05-3L glasses as shown in Figure 4.34c and Figure 4.34d, respectively. The coating thickness is calculated as 980 and 955 nm for TD3-3L and SD05-3L glasses, respectively, which confirms that the coating process was successfully applied for both glasses since similar thickness values result from the same number of layers.

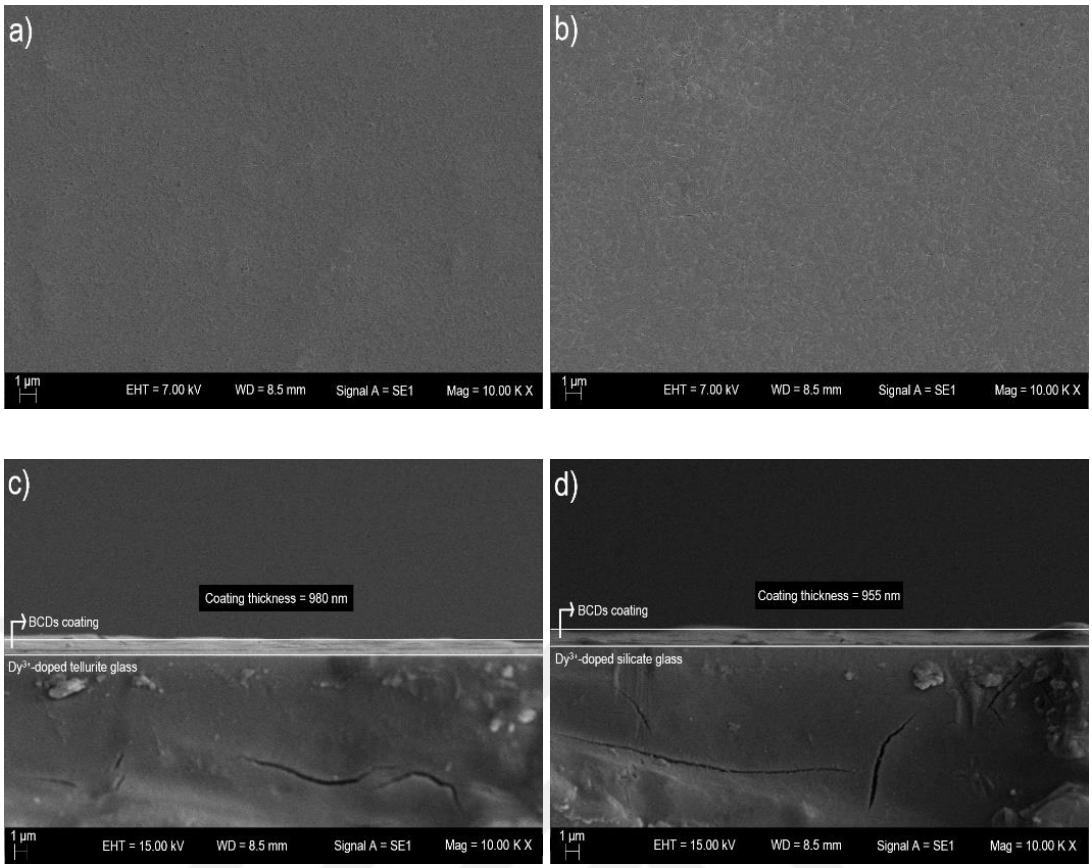


Figure 4.34 The surface and cross-sectional SEM images of a-c) TD3-3L b-d) SD05-3L

For further investigation, several stability analyses are conducted for TD3-3L and SD05-3L glasses since these are the only glasses with white light emission after BCDs-coating. To determine thermal stability of BCDs-coated Dy^{3+}-doped glasses at different temperatures, the thermal stability analysis is performed by recording temperature-dependent PL spectra of TD3–3L and SD05–3L glasses as presented in Figure 4.35a and Figure 4.35b, respectively. The emission intensities of TD3-3L and SD05-3L glasses show no noticeable change even after heating up to 120 °C and glasses maintain approximately 95% of their emission intensities.

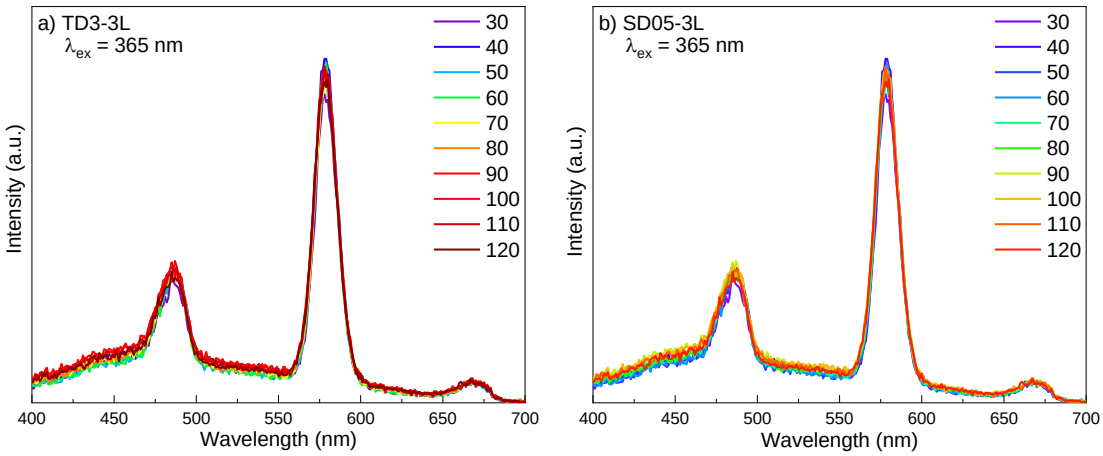


Figure 4.35 Temperature dependent PL spectrum of a) TD3-3L b) SD05-3L glasses under 365 nm excitation

Thermal cycling-dependent PL results of TD3-3L and SD05-3L glasses are given in Figure 4.36a and Figure 4.36b, respectively, to investigate emission intensities after heating up to 120 °C and cooling to 30 °C. The results show that there is no significant change in emission intensities regardless five heating-cooling cycles. The environmentally stable BCDs-coating on the top of a glass, which is durable in various conditions, has consistent PL intensity under high and low temperatures. Also, the nearly sequenced order of the PL intensity confirms that the emission characteristics are almost reversible.

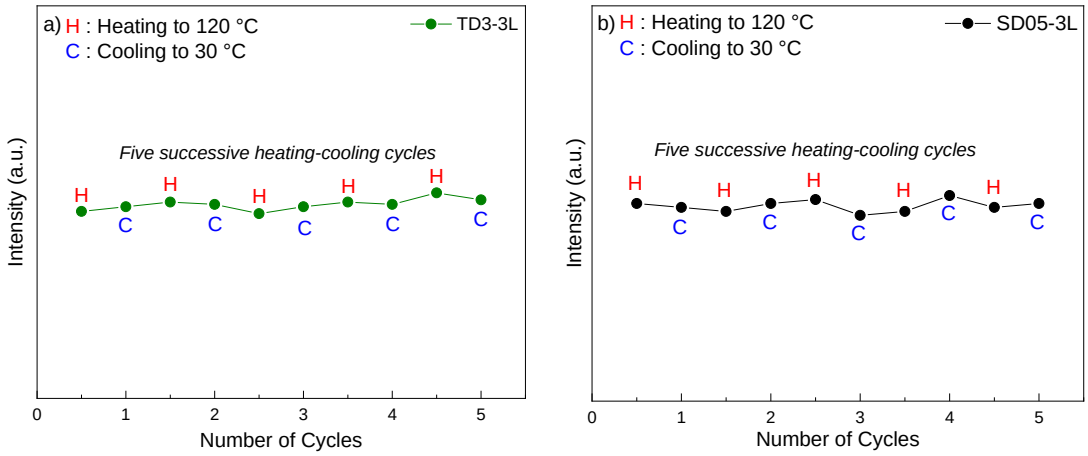


Figure 4.36 Heating-cooling cycles of a) TD3-3L and b) SD05-3L glasses under 365 nm excitation

In addition, to examine the stability of coatings under moist atmospheric conditions, stability measurements are conducted by calculating PLQY results on different days such as 0, 10, 30 and 60. The results are given in Figure 4.37a and Figure 4.37b as a comparison of the PLQY values on selected days. There is no significant change between PLQY values that measured on different days and as it can be seen from Figure 4.37, both glasses continue to hold ~90 % of their initial PLQY value. After 60 days, a slight decrease is observed which can be as a result of unsuitable storage conditions.

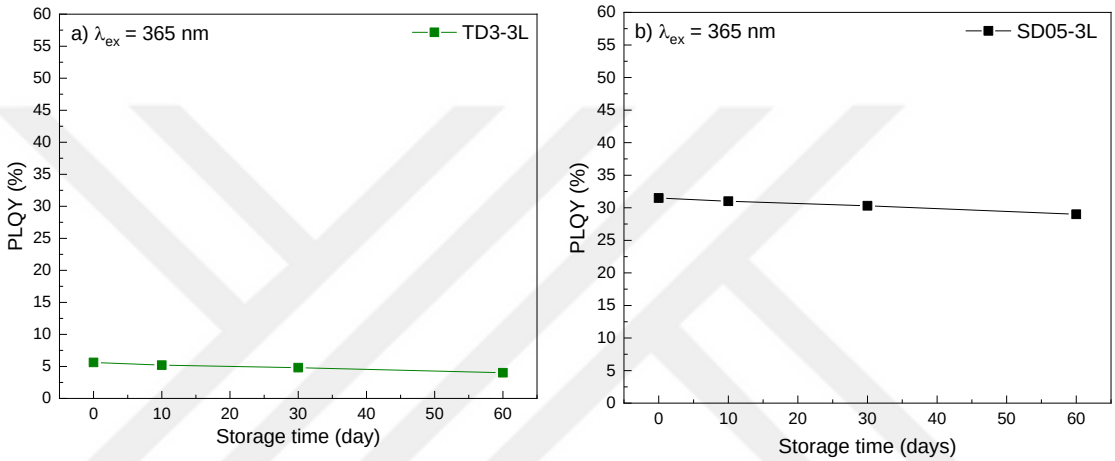


Figure 4.37 Time dependent PLQY spectrum of a) TD3-3L and b) SD05-3L glasses

4.2 Conclusion and Future Outlook

In summary, this thesis concludes a series of experiments to obtain white light emission by combining blue emission from BCDs and yellow emission from Dy^{3+}-doped luminescent glasses. In this approach, Dy^{3+}-doped tellurite and silicate glasses with different Dy^{3+}-ion concentration were synthesized as well as BCDs/PVP solution which applied on the glass surfaces to obtain BCDs-coated glasses. The structural, thermal, optical, and luminescent properties of glasses and BCDs/PVP solution were investigated. Furthermore, several stability studies were conducted for selected glasses with white light emission to consider the potential of BCDs-coated Dy^{3+}-doped glasses to be used in WLED applications in solid-state lighting technologies. The conducted study has yielded several noteworthy findings that shed light on the subject matter, and the following are the key findings that are derived:

- In both tellurite and silicate glass systems, the emission intensity of Dy^{3+}-doped glasses demonstrated a positive correlation with the Dy^{3+} ion concentration, exhibiting an increase as the concentration rises.
- Unlike rare earth ions, carbon dots show broad emission.
- After spin coating three layers of BCDs/PVP solution, BCDs-coating was approximately 1 μm thick and homogeneously distributed on the glass surface.
- Upon 365 nm excitation, the CIE color coordinates of BCD-coated tellurite and silicate glasses shift towards (x = 0.31, y = 0.33) and (x = 0.31, y = 0.34), respectively confirming the achievement of pure white light emission.
- Upon BCD-coating, CCT values changed from neutral to cool white light, CRI values showed approximately a double increase and color purity values exhibited a dramatic decrease.
- After three-layers of BCDs-coating, PLQY values of TD3 and SD05 glasses increased from 3.10% and 20.81% to 5.62 % and 31.49 %, respectively. The PLQY values increased nearly by 50 % for both Dy3+-doped tellurite and silicate glasses.
- The PLQY values of TD3-3L and SD05-3L glasses nearly did not change even after storing for 30 days
- The tellurite and silicate glasses coated with BCDs exhibit remarkable stability across a wide temperature range, making them promising candidates for WLED applications. These BCDs-coated glasses offer enhanced color characteristics compared to conventional materials, further bolstering their suitability as alternative materials in WLED technology.

.

REFERENCES

[1] K. Shahzad, L. Cucek, M. Sagir, N. Ali, M. Rashid, R. Nazir, A. Nizami, H. Al-Turaif, I. Ismail, "An ecological feasibility study for developing sustainable street lighting system," *Journal of Cleaner Production,* vol. 175, pp. 683-695, 2018/02/20/ 2018.

[2] J. Chen, Y. Peng, X. Li, W. Chen, H. Huang, L. Lin, D. Chen, "Near-infrared-laser-driven robust glass-ceramic-based upconverted solid-state-lighting," *Journal of Materials Chemistry C,* 10.1039/C9TC00606K vol. 7, no. 14, pp. 4109-4117, 2019.

[3] X. Zhang, J. Wang, L. Huang, F. Pan, Y. Chen, B. Lei, M. Peng, Mi. Wu, "Tunable Luminescent Properties and Concentration-Dependent, Site-Preferable Distribution of Eu2+ Ions in Silicate Glass for White LEDs Applications," *ACS Applied Materials & Interfaces,* vol. 7, no. 18, pp. 10044-10054, 2015/05/13 2015.

[4] Z. Bi, T. Li, H. Su, Y. Ni, and L. Yan, "Transparent Wood Film Incorporating Carbon Dots as Encapsulating Material for White Light-Emitting Diodes," *ACS Sustainable Chemistry & Engineering,* vol. 6, no. 7, pp. 9314-9323, 2018/07/02 2018.

[5] E. Erol, N. Vahedigharehchopogh, O. Kıbrıslı, M. Ç. Ersundu, and A. E. Ersundu, "Recent progress in lanthanide-doped luminescent glasses for solid-state lighting applications—a review," *Journal of Physics: Condensed Matter,* vol. 33, no. 48, p. 483001, 2021/09/20 2021.

[6] E. Erol, N. Vahedigharehchopogh, U. Ekim, N. Uza, M. Çelikbilek Ersundu, and A. E. Ersundu, "Ultra-stable Eu3+/Dy3+ co-doped CsPbBr3 quantum dot glass nanocomposites with tunable luminescence properties for phosphor-free WLED applications," *Journal of Alloys and Compounds,* vol. 909, p. 164650, 2022/07/15/ 2022.

[7] O. H. Kwon, J. W. Jang, S. J. Park, J. S. Kim, S. J. Hong, Y. S. Jung, H. Yang, Y. J. Kim, Y. S. Cho, "Plasmonic-Enhanced Luminescence Characteristics of Microscale Phosphor Layers on a ZnO Nanorod-Arrayed Glass Substrate," *ACS Applied Materials & Interfaces,* vol. 11, no. 1, pp. 1004-1012, 2019/01/09 2019.

[8] C. Wang, T. Hu, Y. Chen, Y. Xu, and Q. Song, "Polymer-Assisted Self-Assembly of Multicolor Carbon Dots as Solid-State Phosphors for Fabrication of Warm, High-Quality, and Temperature-Responsive White-Light-Emitting Devices," *ACS Applied Materials & Interfaces,* vol. 11, no. 25, pp. 22332-22338, 2019/06/26 2019.

[9] N. Vahedigharehchopogh, O. Kıbrıslı, E. Erol, M. Çelikbilek Ersundu, and A. E. Ersundu, "A straightforward approach for high-end anti-counterfeiting applications based on NIR laser-driven lanthanide doped luminescent glasses," *Journal of Materials Chemistry C,* 10.1039/D0TC05631F vol. 9, no. 6, pp. 2037-2046, 2021.

[10] C. Yu, Z. Yang, A. Huang, Z. Chai, J. Qiu, Z. Song, D. Zhou, "Photoluminescence properties of tellurite glasses doped Dy3+ and Eu3+ for the UV and blue converted WLEDs," *Journal of Non-Crystalline Solids,* vol. 457, pp. 1-8, 2017/02/01/ 2017.

[11] L. Xia, L. Wang, Q. Xiao, Z. Li, W. You, and Q. Zhang, "Preparation and luminescence properties of Eu3+-doped calcium bismuth borate red-light-emitting glasses for WLEDs," *Journal of Non-Crystalline Solids,* vol. 476, pp. 151-157, 2017/11/15/ 2017.

[12] H. Liang, W. Lei, S. Liu, P. Zhang, Z. Luo, and A. Lu, "Color tunable up-conversion luminescence characteristics of Yb3+-Er3+-Tm3+ tri-doped fluorosilicate glass potentially used in WLED field," *Optical Materials,* vol. 119, p. 111320, 2021/09/01/ 2021.

[13] L. Han, J. Song, W. Liu, Z. Xiao, L. Zhang, A. Lu, Z. Xiao, W. You, Q. Zhang, "Preparation and luminescent properties of Tm3+-Dy3+ co-doped phosphate glass for white light-emitting-diode applications," *Journal of Luminescence,* vol. 227, p. 117559, 2020/11/01/ 2020.

[14] O. Kıbrıslı, A. E. Ersundu, and M. Ç. Ersundu, "Dy3+ doped tellurite glasses for solid-state lighting: An investigation through physical, thermal, structural and optical spectroscopy studies," *Journal of Non-Crystalline Solids,* vol. 513, pp. 125-136, 2019/06/01/ 2019.

[15] S. V. Eliseeva, E. V. Salerno, B. A. Lopez Bermudez, S. Petoud, and V. L. Pecoraro, "Dy3+ White Light Emission Can Be Finely Controlled by Tuning the First Coordination Sphere of Ga3+/Dy3+ Metallacrown Complexes," *Journal of the American Chemical Society,* vol. 142, no. 38, pp. 16173-16176, 2020/09/23 2020.

[16] Y. Ruangtaweep, P. Yasaka, J. Rajagukguk, and J. Kaewkhao, "Influence of silver nanoparticles on the Dy3+ luminescence properties in TeO2-ZnO-BaO glasses," *Materials Today: Proceedings,* vol. 5, no. 7, Part 1, pp. 15014-15018, 2018/01/01/ 2018.

[17] V. Kumar, A. Pandey, O. M. Ntwaeaborwa, V. Dutta, and H. C. Swart, "Structural and luminescence properties of Eu3+/Dy3+ embedded sodium silicate glass for multicolour emission," *Journal of Alloys and Compounds,* vol. 708, pp. 922-931, 2017/06/25/ 2017.

[18] M. Shwetha and B. Eraiah, "Influence of Dy3+ions on the physical, thermal, structural and optical properties of lithium zinc phosphate glasses," *Journal of Non-Crystalline Solids,* vol. 555, p. 120622, 2021/03/01/ 2021.

[19] M. Gökçe and D. Koçyiğit, "Spectroscopic investigations of Dy3+ doped borogermanate glasses for laser and wLED applications," *Optical Materials,* vol. 89, pp. 568-575, 2019/03/01/ 2019.

[20] I. C. Pinto, G. Galleani, L. G. Jacobsohn, Y. Ledemi, Y. Messaddeq, and A. S. S. de Camargo, "Fluorophosphate glasses doped with Eu3+ and Dy3+ for X-ray radiography," *Journal of Alloys and Compounds,* vol. 863, p. 158382, 2021/05/15/ 2021.

[21] A. N. Meza-Rocha, A. Speghini, R. Lozada-Morales, and U. Caldiño, "Blue and white light emission in Tm3+ and Tm3+/Dy3+ doped zinc phosphate glasses upon UV light excitation," *Optical Materials,* vol. 58, pp. 183-187, 2016/08/01/ 2016.

[22] C.-F. Wang, R. Cheng, W.-Q. Ji, K. Ma, L. Ling, and S. Chen, "Recognition of Latent Fingerprints and Ink-Free Printing Derived from Interfacial Segregation of Carbon Dots," *ACS Applied Materials & Interfaces,* vol. 10, no. 45, pp. 39205-39213, 2018/11/14 2018.

[23] Y. Zhan, B. Shang, M. Chen, and L. Wu, "One-Step Synthesis of Silica-Coated Carbon Dots with Controllable Solid-State Fluorescence for White Light-Emitting Diodes," *Small,* vol. 15, no. 24, p. 1901161, 2019/06/01 2019.

[24] Y. Zhang, P. Zhuo, H. Yin, Y. Fan, J. Zhang, X. Liu, Z. Chen, "Solid-State Fluorescent Carbon Dots with Aggregation-Induced Yellow Emission for White Light-Emitting Diodes with High Luminous Efficiencies," *ACS Applied Materials & Interfaces,* vol. 11, no. 27, pp. 24395-24403, 2019/07/10 2019.

[25] M. T. Kartal, U. K. Pata, S. Kılıç Depren, and Ö. Depren, "Effects of possible changes in natural gas, nuclear, and coal energy consumption on CO2 emissions: Evidence from France under Russia's gas supply cuts by dynamic ARDL simulations approach," *Applied Energy,* vol. 339, p. 120983, 2023/06/01/ 2023.

[26] Y. Chen, K. Raza, and M. Alharthi, "The nexus between remittances, education, and energy consumption: Evidence from developing countries," *Energy Strategy Reviews,* vol. 46, p. 101069, 2023/03/01/ 2023.

[27] X. Wu, W. Zhang, L. Xie, O. Zhao, Z. Li, J. Li, J. Zhong, "Study on the impact of partition photovoltaic electrochromic windows on building lighting environment and energy saving," *Energy and Buildings,* vol. 280, p. 112722, 2023/02/01/ 2023.

[28] E. F. Schubert and J. K. Kim, "Solid-State Light Sources Getting Smart," *Science,* vol. 308, no. 5726, pp. 1274-1278, 2005/05/27 2005.

[29] Z. Koretsky, "Phasing out an embedded technology: Insights from banning the incandescent light bulb in Europe," *Energy Research & Social Science,* vol. 82, p. 102310, 2021/12/01/ 2021.

[30] M. Zhao, Q. Zhang, and Z. Xia, "Narrow-band emitters in LED backlights for liquid-crystal displays," *Materials Today,* vol. 40, pp. 246-265, 2020/11/01/ 2020.

[31] R. K. Mondal, S. Adhikari, V. Chatterjee, and S. Pal, "Recent advances and challenges in AlGaN-based ultra-violet light emitting diode technologies," *Materials Research Bulletin,* vol. 140, p. 111258, 2021/08/01/ 2021.

[32] T. R. Martins, E. H. Tanabe, and D. A. Bertuol, "Innovative method for the recycling of end-of-life LED bulbs by mechanical processing," *Resources, Conservation and Recycling,* vol. 161, p. 104875, 2020/10/01/ 2020.

[33] G. Liu, S. Zhang, L. Xu, Y. Hu, X. Li, S. Zhang, H. Zeng, "Recent advances of eco-friendly quantum dots light-emitting diodes for display," *Progress in Quantum Electronics,* vol. 86, p. 100415, 2022/09/01/ 2022.

[34] J. Cho, J. H. Park, J. K. Kim, and E. F. Schubert, "White light-emitting diodes: History, progress, and future," *Laser & Photonics Reviews,* vol. 11, no. 2, p. 1600147, 2017/03/01 2017.

[35] N. Vahedigharehchopogh, E. Erol, O. Kıbrıslı, A. Genç, M. Çelikbilek Ersundu, and A. E. Ersundu, "Recyclability of CsPbBr3 quantum dot glass nanocomposites for their long-standing use in white LEDs," *Journal of Materials Chemistry C,* 10.1039/D2TC03568E vol. 10, no. 42, pp. 16088-16099, 2022.

[36] N. Vahedigharehchopogh, O. Kıbrıslı, A. E. Ersundu, and M. Çelikbilek Ersundu, "Color tunability and white light generation through up-conversion energy transfer in Yb3+ sensitized Ho3+/Tm3+ doped tellurite glasses," *Journal of Non-Crystalline Solids,* vol. 525, p. 119679, 2019/12/01/ 2019.

[37] V. Chopra, A. R. Kadam, H. C. Swart, and S. J. Dhoble, "Chapter 1 - Introduction to luminescence and radiation dosimetry techniques," in *Radiation Dosimetry Phosphors*, S. Dhoble, V. Chopra, V. Nayar, G. Kitis, D. Poelman, and H. Swart, Eds.: Woodhead Publishing, 2022, pp. 1-27.

[38] R. Kumar and S. K. Mishra, "11 - Luminescence and photodetection characteristics of rare earth–doped zinc oxide nanostructures," in *Ceramic Science and Engineering*, K. P. Misra and R. D. K. Misra, Eds.: Elsevier, 2022, pp. 263-294.

[39] A. J. Syed and J. C. Anderson, "Applications of bioluminescence in biotechnology and beyond," *Chemical Society Reviews,* 10.1039/D0CS01492C vol. 50, no. 9, pp. 5668-5705, 2021.

[40] M. Yang, J. Huang, J. Fan, J. Du, K. Pu, and X. Peng, "Chemiluminescence for bioimaging and therapeutics: recent advances and challenges," *Chemical Society Reviews*, 10.1039/D0CS00348D vol. 49, no. 19, pp. 6800-6815, 2020.

[41] T. Hu, Y. Gao, B. Wang, T. Yu, D. Wen, Y. Cheng, Q. Zeng, "A new class of battery-free, mechanically powered, piezoelectric Ca5Ga6O14:Tb3+ phosphors with self-recoverable luminescence," *Journal of Materials Chemistry C,* 10.1039/D2TC01554D vol. 10, no. 25, pp. 9554-9562, 2022.

[42] F. Yang, H. Cui, X. Wu, S.-J. Kim, and G. Hong, "Ultrasound-activated luminescence with color tunability enabled by mechanoluminescent colloids and perovskite quantum dots," *Nanoscale,* 10.1039/D2NR06129E vol. 15, no. 4, pp. 1629-1636, 2023.

[43] Y.-C. Duan, L. L. Wen, Y. Gao, L. Zhao, Y. Geng, G. G. Shan, M. Zhang, Z. M. Su, "Fluorescence, Phosphorescence, or Delayed Fluorescence?—A Theoretical Exploration on the Reason Why a Series of Similar Organic Molecules Exhibit Different Luminescence Types," *The Journal of Physical Chemistry C,* vol. 122, no. 40, pp. 23091-23101, 2018/10/11 2018.

[44] N. Siraj, B. E. Zahab, S. Hamdan, T. E. Karam, L. H. Haber, M. Li, S. O. Fakayode, S. Das, B. Valle, R. M. Strongin, G. Patonay, H. O. Sintim, G. A. Baker, A. Powe, M. Lowry, J. O. Karolin, C. D. Geddesi I. M. Warner, "Fluorescence, Phosphorescence, and Chemiluminescence," *Analytical Chemistry,* vol. 88, no. 1, pp. 170-202, 2016/01/05 2016.

[45] Y. Xiao, X. Kuang, Y. Yeung, and M. Ju, "Investigation of the Structure and Luminescence Mechanism of Tm3+-Doped LiYF4: New Theoretical Perspectives," *Inorganic Chemistry,* vol. 59, no. 2, pp. 1211-1217, 2020/01/21 2020.

[46] Y.-Y. Jiang, K. Zhang, M.-S. Zhou, P.-F. Gao, and H.-R. Fu, "A fluorescence/phosphorescence dual-emitting metal-organic framework exhibiting two approaches for single-phase white-light emission," *Journal of Solid State Chemistry,* vol. 304, p. 122563, 2021/12/01/ 2021.

[47] Y. Yu, L. Lan, and H. Cai, "Integrating Down-Shifting and Down-Conversion into Metal–Organic Frameworks to Enhance the Spectral Conversion for Solar Cells," *The Journal of Physical Chemistry C,* vol. 122, no. 1, pp. 96-104, 2018/01/11 2018.

[48] B. Ehrler, N. Yanai, and L. Nienhaus, "Up- and down-conversion in molecules and materials," *The Journal of Chemical Physics,* vol. 154, no. 7, p. 070401, 2021.

[49] O. A. Yeshchenko, I. S. Bondarchuk, V. V. Kozachenko, and M. Y. Losytskyy, "Photoluminescence of rhodamine 6G in plasmonic field of Au nanoparticles: Temperature effects," *Journal of Luminescence,* vol. 158, pp. 294-300, 2015/02/01/ 2015.

[50] J. Yang, M. Fang, and Z. Li, "Organic luminescent materials: The concentration on aggregates from aggregation-induced emission," *Aggregate,* vol. 1, no. 1, pp. 6-18, 2020/12/01 2020.

[51] J. Dong, D. Zhao, Y. Lu, and W.-Y. Sun, "Photoluminescent metal–organic frameworks and their application for sensing biomolecules," *Journal of Materials Chemistry A,* 10.1039/C9TA07022B vol. 7, no. 40, pp. 22744-22767, 2019.

[52] Y. Cui, Y. Yue, G. Qian, and B. Chen, "Luminescent Functional Metal–Organic Frameworks," *Chemical Reviews,* vol. 112, no. 2, pp. 1126-1162, 2012/02/08 2012.

[53] X. Ge, Q. Guo, Q. Wang, T. Li, and L. Liao, "Mineralogical Characteristics and Luminescent Properties of Natural Fluorite with Three Different Colors," *Materials,* vol. 15, no. 6. doi: 10.3390/ma15061983

[54] K. Jiang, S. Sun, L. Zhang, Y. Lu, A. Wu, C. Cai, H. Lin, "Red, Green, and Blue Luminescence by Carbon Dots: Full-Color Emission Tuning and Multicolor Cellular Imaging," *Angewandte Chemie International Edition,* vol. 54, no. 18, pp. 5360-5363, 2015/04/27 2015.

[55] A. Z. M. S. Rahman, "Solid State Luminescent Materials: Applications," in *Reference Module in Materials Science and Materials Engineering*: Elsevier, 2016.

[56] L. Marciniak, K. Kniec, K. Elżbieciak-Piecka, K. Trejgis, J. Stefanska, and M. Dramićanin, "Luminescence thermometry with transition metal ions. A review," *Coordination Chemistry Reviews,* vol. 469, p. 214671, 2022/10/15/ 2022.

[57] C. Wegeberg and O. S. Wenger, "Luminescent First-Row Transition Metal Complexes," *JACS Au,* vol. 1, no. 11, pp. 1860-1876, 2021/11/22 2021.

[58] H. Zhang and H. Zhang, "Special Issue: Rare earth luminescent materials," *Light: Science & Applications,* vol. 11, no. 1, p. 260, 2022/09/02 2022.

[59] G. C. Righini, F. Enrichi, L. Zur, and M. Ferrari, "Rare-earth doped glasses and light managing in solar cells," *Journal of Physics: Conference Series,* vol. 1221, no. 1, p. 012028, 2019/06/01 2019.

[60] L. R. P. Kassab, L. A. Gómez-Malagón, R. M. Gunji, G. R. S. Mattos, J. A. M. Garcia, and C. D. S. Bordon, "(INVITED)Rare-earth ions doped glasses based on TeO2 and GeO2 with and without nanoparticles used as cover to increase Si solar cell performance: A review of recent results," *Optical Materials: X,* vol. 15, p. 100170, 2022/08/01/ 2022.

[61] S. Khan, Y. R. Parauha, D. K. Halwar, and S. J. Dhoble, "Rare Earth (RE) doped color tunable phosphors for white light emitting diodes," *Journal of Physics: Conference Series,* vol. 1913, no. 1, p. 012017, 2021/05/01 2021.

[62] J. R. DiMaio, B. Kokuoz, and J. Ballato, "White light emissions through down-conversion of rare-earth doped LaF3 nanoparticles," *Optics Express,* vol. 14, no. 23, pp. 11412-11417, 2006/11/13 2006.

[63] C.-h. Bae and K.-S. Lim, "Enhanced Blue Emission in Er3+/Yb3+ Doped Glass-ceramics Containing Ag Nanoparticles and ZnO Nanocrystals," *Current Optics and Photonics,* vol. 3, no. 2, pp. 135-142, 2019/04/25 2019.

[64] Y. Lu, H. Cheng, P. S. Francis, and Y. Zheng, "Chapter 13 - Nanomaterials and artificial intelligence in anti-counterfeiting," in *Intelligent Nanotechnology*, Y. Zheng and Z. Wu, Eds.: Elsevier, 2023, pp. 361-398.

[65] I. Nelli, A. M. Kaczmarek, F. Locardi, V. Caratto, G. A. Costa, and R. Van Deun, "Multidoped Ln3+ gadolinium dioxycarbonates as tunable white light emitting phosphors," *Dalton Transactions,* 10.1039/C6DT04629K vol. 46, no. 9, pp. 2785-2792, 2017.

[66] A. Hooda, S. P. Khatkar, A. Khatkar, S. Chahar, S. Devi, J. Dalal, V. B. Taxak, "Characteristic white light emission via down-conversion SrGdAlO4:Dy3+ nanophosphor," *Current Applied Physics,* vol. 19, no. 5, pp. 621-628, 2019/05/01/ 2019.

[67] N. Jaidass, C. Krishna Moorthi, A. Mohan Babu, and M. Reddi Babu, "Luminescence properties of Dy3+ doped lithium zinc borosilicate glasses for photonic applications," *Heliyon,* vol. 4, no. 3, p. e00555, 2018/03/01/ 2018.

[68] S. Kaur, A. K. Vishwakarma, N. Deopa, A. Prasad, M. Jayasimhadri, and A. S. Rao, "Spectroscopic studies of Dy3+ doped borate glasses for cool white light generation," *Materials Research Bulletin,* vol. 104, pp. 77-82, 2018/08/01/ 2018.

[69] K. Mariselvam and J. Liu, "Down-conversion luminescence and shielding parameters of Dy3+: NFBT glass for white LED and radiation applications," *Optical Materials,* vol. 114, p. 110997, 2021/04/01/ 2021.

[70] A. R. Kadam and S. J. Dhoble, "Energy transfer mechanism of KAlF4:Dy3+, Eu3+ co-activated down-conversion phosphor as spectral converters: An approach towards improving photovoltaic efficiency by downshifting layer," *Journal of Alloys and Compounds,* vol. 884, p. 161138, 2021/12/05/ 2021.

[71] N. Shasmal and B. Karmakar, "White light-emitting Dy3+-doped transparent chloroborosilicate glass: synthesis and optical properties," *Journal of Asian Ceramic Societies,* vol. 7, no. 1, pp. 42-52, 2019/01/02 2019.

[72] W. Rittisut, N. Wantana, Y. Ruangtaweep, P. Moolamkha, J. Padchasri, S. Rujirawat, P. Manyum, R. Yimnirun, P. Kidkhunthod, A. Prasatkhetragarn, S. Kothan, H. J. Kim, J. Kaewkhao, "Bright white light emission from (Gd3+ /Dy3+)

dual doped transparent lithium aluminum borate glasses for W- LED application," *Optical Materials,* vol. 122, p. 111705, 2021/12/01/ 2021.

[73] X. Chen, A. V. Khamenok, S. G. Khusainov, M. V. Shestakov, and V. V. Moshchalkov, "White Photoluminescence in Dy-Doped Oxyfluoride Glasses," *Optics*, vol. 4, no. 1, pp. 66-73. doi: 10.3390/opt4010006

[74] S. Liu, G. Zhao, X. Lin, H. Ying, J. Liu, J. Wang, G. Han, "White luminescence of Tm–Dy ions co-doped aluminoborosilicate glasses under UV light excitation," *Journal of Solid State Chemistry,* vol. 181, no. 10, pp. 2725-2730, 2008/10/01/ 2008.

[75] Z. Tian, X. Zhang, D. Li, D. Zhou, P. Jing, D. Shen, S. Qu, R. Zboril, A. L. Rogach, "Full-Color Inorganic Carbon Dot Phosphors for White-Light-Emitting Diodes," *Advanced Optical Materials,* vol. 5, no. 19, p. 1700416, 2017/10/01 2017.

[76] H. Yi, J. Liu, J. Yao, R. Wang, W. Shi, and C. Lu, "Photoluminescence Mechanism of Carbon Dots: Triggering Multiple Color Emissions through Controlling the Degree of Protonation," *Molecules,* vol. 27, no. 19. doi: 10.3390/molecules27196517

[77] F. Yan, Z. Sun, H. Zhang, X. Sun, Y. Jiang, and Z. Bai, "The fluorescence mechanism of carbon dots, and methods for tuning their emission color: a review," *Microchimica Acta,* vol. 186, no. 8, p. 583, 2019/07/29 2019.

[78] Z. Chen, R. Zhou, J. Cui, H. Yan, and L. Li, "Fabrication of fluorescent carbon dots by laser ablation in alkaline solution coupled with Ag nanoparticles for enhanced SERS," *MRS Communications,* vol. 11, no. 4, pp. 489-497, 2021/08/01 2021.

[79] M. Liu, Y. Xu, F. Niu, J. J. Gooding, and J. Liu, "Carbon quantum dots directly generated from electrochemical oxidation of graphite electrodes in alkaline alcohols and the applications for specific ferric ion detection and cell imaging," *Analyst,* 10.1039/C5AN02231B vol. 141, no. 9, pp. 2657-2664, 2016.

[80] A. Chae, Y. Choi, S. Jo, Nur'aeni, P. Paoprasert, S. Y. Park, I. In, "Microwave-assisted synthesis of fluorescent carbon quantum dots from an A2/B3 monomer set," *RSC Advances,* 10.1039/C6RA28176A vol. 7, no. 21, pp. 12663-12669, 2017.

[81] H. Shibata, M. Abe, K. Sato, K. Uwai, K. Tokuraku, and T. Iimori, "Microwave-assisted synthesis and formation mechanism of fluorescent carbon dots from starch," *Carbohydrate Polymer Technologies and Applications,* vol. 3, p. 100218, 2022/06/01/ 2022.

[82] Y. Wang, Y. Zhu, S. Yu, and C. Jiang, "Fluorescent carbon dots: rational synthesis, tunable optical properties and analytical applications," *RSC Advances,* 10.1039/C7RA07573A vol. 7, no. 65, pp. 40973-40989, 2017.

[83] B. Han, X. Hu, X. Zhang, X. Huang, M. An, X. Chen, D. Zhao, J. Li, "The fluorescence mechanism of carbon dots based on the separation and identification of small molecular fluorophores," *RSC Advances,* 10.1039/D2RA00431C vol. 12, no. 19, pp. 11640-11648, 2022.

[84] X. Miao, D. Qu, D. Yang, B. Nie, Y. Zhao, H. Fan, Z. Sun, "Synthesis of Carbon Dots with Multiple Color Emission by Controlled Graphitization and Surface

Functionalization," *Advanced Materials,* vol. 30, no. 1, p. 1704740, 2018/01/01 2018.

[85] S. Zhu, Y. Song, X. Zhao, J. Shao, J. Zhang, and B. Yang, "The photoluminescence mechanism in carbon dots (graphene quantum dots, carbon nanodots, and polymer dots): current state and future perspective," *Nano Research,* vol. 8, no. 2, pp. 355-381, 2015/02/01 2015.

[86] L. Ai, Y. Yang, B. Wang, J. Chang, Z. Tang, B. Yang, S. Lu, "Insights into photoluminescence mechanisms of carbon dots: advances and perspectives," *Science Bulletin,* vol. 66, no. 8, pp. 839-856, 2021/04/30/ 2021.

[87] Q. Zhang, R. Wang, B. Feng, X. Zhong, and K. Ostrikov, "Photoluminescence mechanism of carbon dots: triggering high-color-purity red fluorescence emission through edge amino protonation," *Nature Communications,* vol. 12, no. 1, p. 6856, 2021/11/25 2021.

[88] H. Yang, Y. Liu, Z. Guo, B. Lei, J. Zhuang, X. Zhang, Z. Liu, C. Hu, "Hydrophobic carbon dots with blue dispersed emission and red aggregation-induced emission," *Nature Communications,* vol. 10, no. 1, p. 1789, 2019/04/17 2019.

[89] X. Wang, X. Teng, X. Sun, W. Pan, and J. Wang, "Carbon dots with aggregation induced quenching effect and solvatochromism for the detection of H2O in organic solvents," *Spectrochimica Acta Part A: Molecular and Biomolecular Spectroscopy,* vol. 267, p. 120547, 2022/02/15/ 2022.

[90] P. Wang, W. Zhang, and S.-Q. Man, "Synthesis, structure and photoluminescence properties of Tm3+/Dy3+ co-doped borate glass for near-UV white LEDs," *Ceramics International,* vol. 49, no. 7, pp. 10428-10436, 2023/04/01/ 2023.

[91] L. Vijayalakshmi, K. Naveen Kumar, and J. D. Baek, "Cool white light and tunable multicolor emission from Tb3+/Dy3+ co-activated glasses under different excitations for WLEDs," *Journal of Rare Earths,* 2022/11/18/ 2022.

[92] L.-y. Fang and J.-t. Zheng, "Carbon quantum dots: Synthesis and correlation of luminescence behavior with microstructure," *New Carbon Materials,* vol. 36, no. 3, pp. 625-631, 2021/06/01/ 2021.

[93] Y. An, C. Liu, Y. Li, M. Chen, Y. Zheng, H. Tian, R. Shi, X. He, X. Lin, "Preparation of Multicolour Solid Fluorescent Carbon Dots for Light-Emitting Diodes Using Phenylethylamine as a Co-Carbonization Agent," *International Journal of Molecular Sciences,* vol. 23, no. 19. doi: 10.3390/ijms231911071

[94] S. Xu, F. Jia, G. Zhang, T. Zhao, H. Zhang, and C. Su, "Preparation and luminescence properties of Dy3+ doped BaO-Al2O3-SiO2 glass ceramics," *Journal of Non-Crystalline Solids,* vol. 581, p. 121436, 2022/04/01/ 2022.

[95] M. M. Rodríguez-García, J. A. G. Williams, and I. R. Evans, "Single-phase white-emitting phosphors based on apatite-type gadolinium silicate, Gd9.33(SiO4)6O2 doped with Dy3+, Eu3+ and Tb3+," *Journal of Materials Chemistry C,* 10.1039/C9TC02336D vol. 7, no. 25, pp. 7779-7787, 2019.

[96] X. Wang, X. Shi, M. S. Molokeev, Z. Wang, Q. Zhu, X. Li, X. Sun, J. G. Li, "NaLaW2O7(OH)2(H2O): Crystal Structure and RE3+ Luminescence in the Pristine and Annealed Double Tungstates (RE = Eu, Tb, Sm, and Dy)," *Inorganic Chemistry,* vol. 57, no. 21, pp. 13606-13617, 2018/11/05 2018.

[97] B. Ding, C. Yu, H. Xin, Z. Li, H. Yu, J. Xu, Z. Zhao, H. Zheng, J. Zhang, S. Zheng, Y. Han, "Effect of Dy3+ and Eu3+ 4f Band Gap States on Luminescence and Energy Transfer in Monoclinic Lutetium Tungstate," *ACS Applied Electronic Materials,* vol. 1, no. 5, pp. 772-782, 2019/05/28 2019.

[98] H. Guan, Y. Song, P. Ma, M. Chang, J. Chen, Y. Wang, B. Yuan, H. Zou, "Magnetic-downconversion luminescent bifunctional BaGdF5:Dy3+,Eu3+ nanospheres: energy transfer, multicolor luminescence and paramagnetic properties," *RSC Advances,* 10.1039/C6RA09754E vol. 6, no. 58, pp. 53444-53453, 2016.

[99] A. Fujimoto, Y. Yamada, M. Koinuma, and S. Sato, "Origins of sp3C peaks in C1s X-ray Photoelectron Spectra of Carbon Materials," *Analytical Chemistry,* vol. 88, no. 12, pp. 6110-6114, 2016/06/21 2016.

[100] Y. Ding, F. Zhang, J. Xu, Y. Miao, Y. Yang, X. Liu, B. Xu, "Synthesis of short-chain passivated carbon quantum dots as the light emitting layer towards electroluminescence," *RSC Advances,* 10.1039/C7RA02421E vol. 7, no. 46, pp. 28754-28762, 2017.

[101] W.-B. Zhao, K.-K. Liu, S.-Y. Song, R. Zhou, and C.-X. Shan, "Fluorescent Nano-Biomass Dots: Ultrasonic-Assisted Extraction and Their Application as Nanoprobe for Fe3+ detection," *Nanoscale Research Letters,* vol. 14, no. 1, p. 130, 2019/04/15 2019.

[102] M. Ö. Alaş and R. Genç, "Solvatochromic Surface-Passivated Carbon Dots for Fluorometric Moisture Sensing in Organic Solvents," *ACS Applied Nano Materials,* vol. 4, no. 8, pp. 7974-7987, 2021/08/27 2021.

[103] Y.-Y. Chen, W. P. Jiang, H. L. Chen, H. C. Huang, G. J. Huang, H. M. Chiang, C. C. Chang, C. L. Huang, T. Y. Juang, "Cytotoxicity and cell imaging of six types of carbon nanodots prepared through carbonization and hydrothermal processing of natural plant materials," *RSC Advances,* 10.1039/D1RA01318A vol. 11, no. 27, pp. 16661-16674, 2021.

[104] Q. Zhang, C.-F. Wang, L.-T. Ling, and S. Chen, "Fluorescent nanomaterial-derived white light-emitting diodes: what's going on," *Journal of Materials Chemistry C,* 10.1039/C4TC00048J vol. 2, no. 22, pp. 4358-4373, 2014.

[105] L. Zhou, P. Du, W. Li, and L. Luo, "Lithium ion doping triggered splendid quantum efficiency and thermal stability in Li2SrSiO4:xEu2+ phosphors for optical thermometry and high luminous efficiency white-LED," *New Journal of Chemistry,* 10.1039/C9NJ04102H vol. 43, no. 42, pp. 16445-16453, 2019.

PUBLICATIONS FROM THE THESIS

Papers

1. B. Ozlem, U. Korkmaz, E. Erol, M. Ö. Alaş, Z. Meray, R. G. Altürk, M. Ç. Ersundu, A. E. Ersundu, "Bright white light emission from blue emitting carbon dot-coated Dy^{3+}-doped luminescent glasses", *Journal of Alloys and Compounds*, vol. 926, 166763, 2022.

Projects

1. The Scientific and Technological Research Council of Turkey (TUBITAK) – Research Project No: 119C025 "*The development of new generation luminescent glasses for solid state lighting systems*", Research Scholar, (2020-2022)

2. YTU Scientific Research Project (BAP) No: FBA-2022-4999 "*The development of photoluminescent properties of blue emitting carbon dots coated luminescent glasses for solid-state lighting technologies*", Researcher, (2020-2022)